REPORT DOCUMENTATION PAGE

Public reporting burden for this collection of information is estimated to average 1 hour per response, including the time for reviewing instructions, searching existing data sources, gathering and maintaining the data needed, and completing and reviewing the collection of information. Send comments regarding this burden estimate or any other aspect of this collection of information, including suggestions for reducing this burden, to Washington Headquarters Services, Directorate for Information Operations and Reports, 1215 Jefferson Davis Highway, Suite 1204, Arlington, VA 22202-4302, and to the Office of Management and Budget, Paperwork Reduction Project (0704-0188), Washington, DC 20503.

1. AGENCY USE ONLY (Leave blank)	2. REPORT DATE February 17, 1997	3. REPORT TYPE AND DATES COVERED Technical 9/1/94 - 3/31/97

4. TITLE AND SUBTITLE
Kilo-Constant-Current Anemometer System for Surface Hot-films in Water

5. FUNDING NUMBERS
N00014-91-J-1732-P07

6. AUTHOR(S)
Todd G. Wetzel, Roger L. Simpson, and Jonathan L. Fleming

7. PERFORMING ORGANIZATION NAME(S) AND ADDRESS(ES)
Virginia Polytechnic Institute and State University
Aerospace and Ocean Engineering Department
215 Randolph Hall
Blacksburg, VA 24061-0203

8. PERFORMING ORGANIZATION REPORT NUMBER
VPI-AOE-226

9. SPONSORING/MONITORING AGENCY NAME(S) AND ADDRESS(ES)
Office of Naval Research
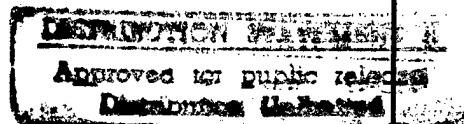800 N. Quincy St.
Arlington, VA 22217

10. SPONSORING/MONITORING AGENCY REPORT NUMBER

19970327 068

11. SUPPLEMENTARY NOTES

12a. DISTRIBUTION/AVAILABILITY STATEMENT

Unlimited

DISTRIBUTION STATEMENT A
Approved for public release
Distribution Unlimited

12b. DISTRIBUTION CODE

13. ABSTRACT (Maximum 200 words)

A system for measuring the 3-D separation topology as a large scale underwater submarine model is described. Magnitude-only hot-film sensors are powered by constant current anemometers. The system is designed to use over 1000 sensors. Minima in skin friction magnitude are used to indicate crossflow separation. The hardware and sensor installation is described along with the result of several tests at the David Taylor Research Center's Rotating Arm facility. Future improvements are discussed along with a detailed uncertainty analysis to guide future designs.

14. SUBJECT TERMS
Hotfilm sensors; Anemometers; Separation; Fluid Dynamics; water flow

15. NUMBER OF PAGES
77

16. PRICE CODE

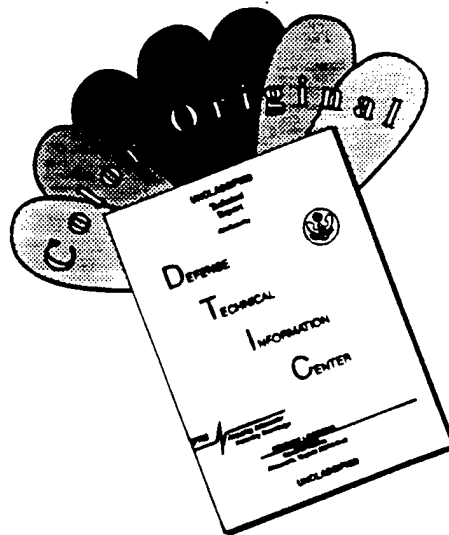| 17. SECURITY CLASSIFICATION OF REPORT	18. SECURITY CLASSIFICATION OF THIS PAGE	19. SECURITY CLASSIFICATION OF ABSTRACT	20. LIMITATION OF ABSTRACT
Unclassified	Unclassified	Unclassified	Unlimited

DISCLAIMER NOTICE

Table of Contents

Nomenclature

A_s sensor area

C_f skin friction coefficient, τ_w/q_∞

c_p specific heat

d sensor diameter

h heat transfer film coefficient; OR trip post height

I current

k or thermal conductivity

l sensor length

M constant

n number of currents used

P pressure

$\dot{q}$ heat transfer

q_∞ dynamic pressure, $\frac{1}{2}\rho U_\infty^{\,2}$

r correlation coefficient; OR local radial distance in flow from model axis

R_{cold} reference (cold) resistance at free-stream temperature

R_{curr} current-sensing resistance

Re Reynolds number, $U_\infty L/\nu$

R_L total lead resistance

R_{L1}, R_{L2} component lead resistances

R_o cold resistance at the reference temperature

R_s sensor resistance

St Stanton number

T temperature

T_{cold} cold resistance reference temperature

T_f foil temperature

T_w wall temperature

T_o free-stream temperature

U_∞ free-stream velocity

V wall normal velocity

V_1, V_2 constant temperature measured voltages

V_s sensor voltage

w sensor width

y wall normal coordinate

α	thermal coefficient of resistivity; OR thermal diffusivity
δ	uncertainty
μ	viscosity
Θ	sensor temperature difference, $T_f\text{-}T_\infty$
σ_q^2	heat transfer variance
σ_Θ^2	temperature difference variance
ρ	air density
τ_w	wall shear force

Introduction

Separation topologies on submarine configurations are difficult to measure on underwater models. It was desired to develop some transducer-based system to provide for rapid on-line measurement of this topology since hull flow separation plays such a dominant role in submarine hydrodynamics. A 1000-sensor constant-current anemometer system that was designed and implemented to fill this task is described in detail in this report. Custom sensors and electronics were built and interfaced to a personal computer. 980 sensors were installed on a 20' long submarine model, and several attempts were made to measure the flow separation. This first-generation system did not succeed in measuring separation locations on the model under water, but did provide a wealth of knowledge that is necessary for any future attempts to be successful. This report describes the sensor theory and operation, and then documents in detail the hardware and software that were implemented for this system. Then a chronological account of the work performed in this project is described, including the two entries at the Model Basin and the numerous tests and labor performed at Virginia Tech. After making specific hardware-related suggestions for improvement, the sensor design is revisited, with due regard for the experiences gathered during this project. In this final section sensor performance and *measurement uncertainties* are linked to the sensor and anemometer design. This last section provides a starting point from which any other similar anemometer work should proceed. This report does not seek to mandate future directions, but rather to relate the experiences from the present project and provide options for future directions for this work.

Sensor Design: Implementation in Water

Theory of Operation

The surface skin-friction was measured with the hot film sensors designed and documented by Simpson et. al.(1991). The sensors work by heating the near-wall fluid through forced convection. Due to the similarity between gradient transport of momentum and scalars (heat), the amount of heat transfer into the fluid gives a measure of the wall shear. Simpson et. al.(1991) provide an analysis for the operation of the sensor by assuming forced convection into a high Prandtl number fluid. They show that the mean film coefficient $\overline{h}$ is proportional to the cube root of the near-wall velocity gradient, which is thus proportional to the wall shear:

$$\overline{h} = \frac{\dot{\overline{q}}}{lw(T_w - T_{cold})} = \frac{3}{2}Mk\frac{(\partial U/\partial y)_w^{1/3}}{(3\alpha l)^{1/3}}$$

$$\tau_w = \mu\frac{\partial U}{\partial y} \propto \overline{h}^3$$

In this relation, $\dot{\overline{q}}$ is the time-mean heat transfer into the fluid, T_w is the wall (sensor) temperature, T_{cold} is the free-stream temperature, M is a constant (1.12), k is the thermal conductivity, l and w describe the sensor size, α is the thermal diffusivity, and μ is the viscosity. The main purpose of the sensors is not necessarily to measure the absolute magnitude of the wall shear or the skin friction coefficient, but to more importantly measure the relative shear distributions, through measurements of the film coefficient, to allow the researcher the ability to locate shear minima and thus separation locations. However, wall shear magnitudes are possible with adequate calibration. In the same work, Simpson et. al.(1991) show that the wall shear provides higher order information about the separation location than pressure by arguing that three-dimensional separations are characterized by high wall-normal velocity (V) components. By analyzing the continuity and momentum equations near the wall, Simpson et. al.(1991) showed that

$$V = -\frac{1}{2\mu}(\nabla\cdot\vec{\tau}_w)y^2 + \frac{1}{6\mu}(\nabla^2 P)y^3 + \cdots$$

Thus, separation locations, which are locations of high wall-normal velocity V, are characterized by wall shear minima.

Constant current anemometers are used in steady tests to operate the hot film sensors. A voltage-controlled current is supplied to a string of sensors that are connected in series. The voltage drop across the sensor is sampled as a measurement of the change in resistance of the sensor foil. The heat transfer is then obtained by assuming that all of the Joule heating in the sensor is transferred to the fluid (no heat transfer to the substrate):

$$\dot{q} = I^2 R_s = hA_s(T_f - T_{cold})$$

where I is the sensor current, R_s is the sensor resistance, T_f is the foil temperature, and T_{cold} is the free-stream temperature. The foil temperature is determined from the change in resistance relative to a known "cold" resistance at a know temperature:

$$(T_f - T_{cold}) = \frac{1}{\alpha} \left(\frac{R_s}{R_{cold}} - 1 \right)$$

where α is the temperature coefficient of resistivity, and R_{cold} is the sensor resistance at T_{cold}.

The Sensors

The sensors used are shown in Figure 1. They consist primarily of a spiral 5.1 mm in diameter. This corresponds to d/L=0.004 longitudinally, 2.5° wide at the model center, and 3.9° wide at the extreme sensor locations. The spiral shape results in a directional sensitivity of as much as +/-5% (see Wetzel, 1996). This design of hot film sensor is intended for measuring shear magnitude only, and not shear direction. The sensors are made of Balco foil (70% nickel, 30% iron) with a nominal temperature coefficient of resistivity of 0.0051/°C. The foil sensor is bonded to a Kapton substrate. The total sensor thickness is 0.0635 mm. These particular sensors were manufactured by MINCO, Inc., and can be placed in any array or configuration. The sensors were glued to the fiberglass model using Micro Measurements M-BOND 200 strain gage adhesive. The sensors are connected in series with 0.0254 mm thick copper foil that is soldered to the contact pads on the sensors.

Actual Size

5X Size

All Dim.'s in mm.
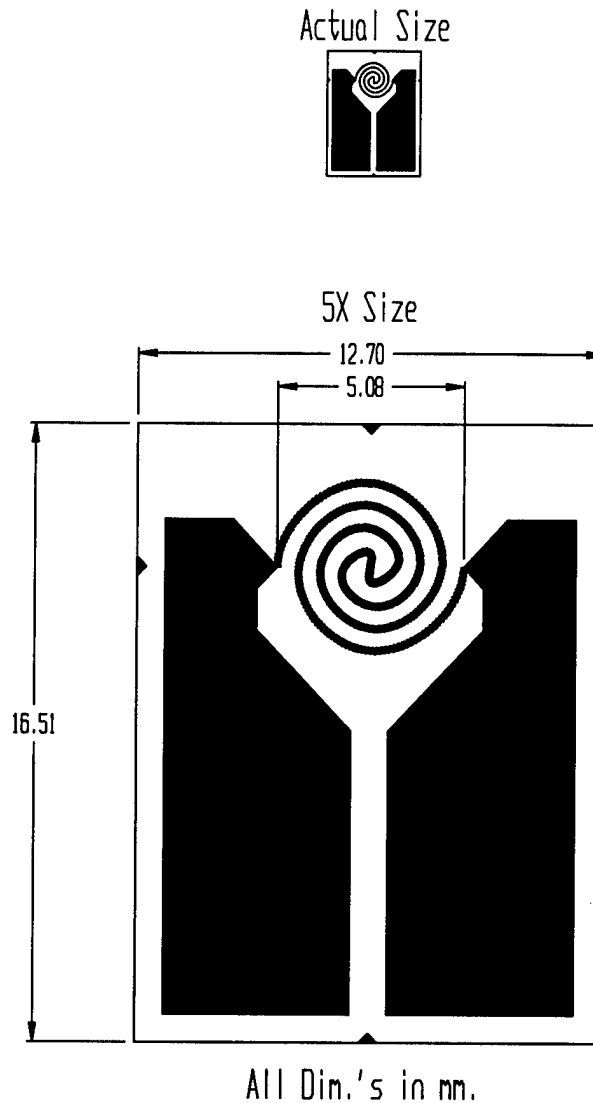
Figure 1. Sensor geometry.

Experimental Apparatus

The constant current hot-film anemometers are diagrammed in Figure 2. Each anemometer board can handle up to 128 sensors. Up to 32 sensors are connected in series with one of four voltage-controlled current sources that are hooked up to a D/A line from the Analogic HSDAS-16 data acquisition board. Leads from each sensor are connected to the inputs of a differential amplifier with a gain set by interchanging resistor chips on the anemometer board. The output of the amplifiers, in groups of 16, are fed into one of eight 16-channel multiplexers. Finally, the output of each multiplexer is fed to an A/D line on the data acquisition board, which is installed inside a PC computer. A CTRTM-10 counter-timer board installed in the PC is hooked up to the multiplexers and the data acquisition card to automatically sequence the multiplexers and synchronize data acquisition.

Figure 2. Constant Current Anemometer block diagram.

It was found that the current sources on the anemometer boards are very linear if a quick calibration is performed, but if the anemometers are left on for long periods of time (20 seconds or more) at high currents,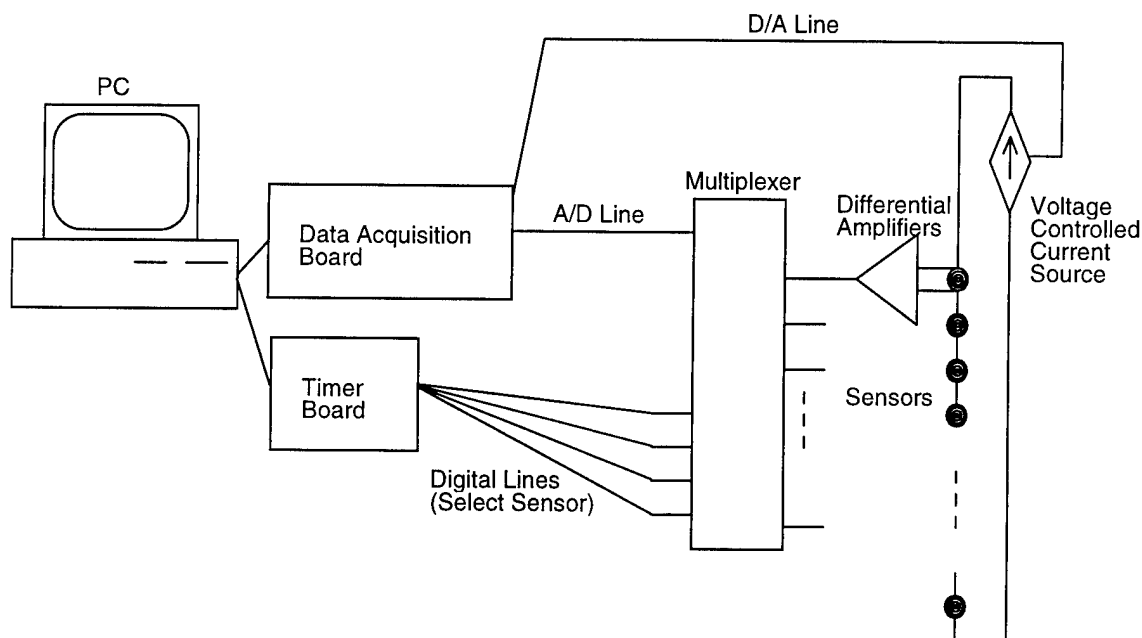 the output current tends to drift by as much as several milliamps. A precision (+/-0.05%) resistor was hard-wired in series with the sensor string as sensor 32. This provided a direct measurement of the sensor current.

Data Reduction and Uncertainties

The data reduction scheme intended for the current system is described below along with a detailed uncertainty analysis. This is an identical reduction and uncertainty analysis as used in Wetzel (1996). Also note that it was this uncertainty analysis which was used at the model basin to determine the lack of sensitivity of the system in water.

Fundamental Quantities

Several fundamental quantities are measured that are used to compute the film coefficient and ultimately the wall shear. The computer data acquisition and control system place easily documented unknowns on both the sensor current and voltage. The current is set with a 12 bit DAC that has an output range of +10V. The current has a gain of 50 mA/V. The current sources drift at high currents as they overheat, so the current source output is monitored with a very high precision resistor (2.5Ω+/-0.05%) and one of the 16-bit A/D lines. This results in an effective current source resolution of 0.1 mA, or 0.03% full scale.

The sensor voltage is amplified with a differential amplifier that is set to a nominal gain of 10. Each amplifier is calibrated against precision resistors (2.5Ω+/-0.05%) and the current source monitor calibration (+/-

0.03%) to determine each amplifier offset and gain. The 16-bit ADC is set with a 0-10V range, resulting in 0.15 mV bit noise. The electronic noise has been found to be roughly 0.5 to 1.0 mV. Due to the extremely good linearity and repeatability of the amplifier calibrations (R^2 typically 0.99999 for a given least-squares calibration), the sensor voltage uncertainty is assumed to be due only to electronic noise. Therefore, the sensor voltage uncertainty is (1.0 mV)/(gain of 10) or 100 μV, or 0.01% full scale.

The other fundamental quantities that are measured are the sensor coefficient of resistivity, α, and the cold resistance of each sensor. The coefficient of resistivity was not determined experimentally. This uncertainty is much less critical since the same value of α is used for all calculations. Thus, this uncertainty will affect all measurements equally, which may increase the absolute wall shear uncertainty but will have no effect on the relative wall shear uncertainty between any two sensors. A value of 0.0051 $°K^{-1}$ is used, which is the supplied value for BALCO foil.

The cold resistance of each sensor is first measured at some known temperature. The cold resistance is calculated from:

$$R_{cold} = R_0 \left[1 - \alpha (T_{cold} - T_0) \right]$$

The cold resistance uncertainty relation is:

$$\delta R_{cold}^2 = \left\{ \begin{array}{l} \left[1 + \alpha (T_{cold} - T_0) \right]^2 \delta R_0^2 + R_0^2 (T_{cold} - T_0)^2 \delta \alpha^2 \\ + R_0^2 \alpha^2 (\delta T_{cold}^2 + \delta T_0^2) \end{array} \right\}^2$$

The uncertainty of primary concern here is the temperature measurement uncertainty, since the resistance can be measured to within 0.2% and thermal coefficient of resistivity uncertainty is negligible. To establish the relative uncertainty required on the temperature, it is desired to force the temperature uncertainty contribution of the cold resistance uncertainty to the same order of magnitude as the other uncertainty terms ("balance of uncertainties"). The first uncertainty term is the dominating one. Also, it is assumed that the two temperature uncertainties are identical, since they are measured with the same transducer. Then, these two uncertainty terms can be equated to determine the required temperature uncertainty:

$$\left[1 + \alpha (T_{cold} - T_0) \right]^2 \delta R_0^2 = 2 R_0^2 \alpha^2 \delta T^2$$

$$\delta T^2 = \frac{\delta R_0^2}{R_0^2} \frac{\left[1 + \alpha (T_{cold} - T_0) \right]^2}{2 \alpha^2}$$

$$= \frac{1}{2} \frac{\delta R_0^2}{R_0^2} \left[\frac{1}{\alpha^2} + 2 \frac{T_{cold} - T_0}{\alpha} + (T_{cold} - T_0)^2 \right]$$

Using the estimate that the relative resistance uncertainty is 0.2% and the thermal coefficient of resistivity is 0.0051/$°K$, this uncertainty becomes:

$$\delta T^2 = \frac{1}{2}(0.002)^2\left[\frac{1}{0.0051^2} + 2\frac{T_{cold} - T_0}{0.0051} + \left(T_{cold} - T_0\right)^2\right]$$

$$= 0.076 + 8\times10^{-4}\left(T_{cold} - T_0\right) + 5\times10^{-7}\left(T_{cold} - T_0\right)^2$$

$$\approx 0.076$$

$$so\ \delta T \approx 0.28\ °C$$

In this approximation, it was assumed that the temperature difference would be less than 50°C. Therefore, the temperature measurement must be accurate to within roughly 0.1°C. When measuring the cold resistance and the water temperature, a glass thermometer was used with a resolution of 0.05°C.

Measuring the cold resistance can be very difficult. It was found that the sensor resistance can drift significantly just due to breezes in the room or even the body temperature of a person holding probes on a sensor. To maximize the accuracy of the cold resistance readings, blocks of foam rubber were taped over the sensors in order to damp out any local temperature fluctuations imposed by the environment. A calibrated, high precision HP 3478A Multimeter was used in four-wire resistance mode to measure the cold resistances down to 0.005 Ω, or roughly 0.2% full scale.

Sensor Temperature and Heat Transfer

Heat transfer is computed from the sensor voltage and sensor current, thus:

$$\dot{q} = V_s I$$

In relative terms, this uncertainty can be expressed as

$$\frac{\delta \dot{q}}{\dot{q}} = \sqrt{\left(\frac{\delta V_s}{V_s}\right)^2 + \left(\frac{\delta I}{I}\right)^2}$$

which indicates that the heat transfer uncertainty will be dominated by the lower resolution of the current sources, or 0.15% full scale.

The temperature difference Θ is computed from:

$$\Theta = \frac{1}{\alpha}\left(\frac{V_s}{IR_{cold}} - 1\right)$$

Its uncertainty is

$$\delta\Theta = \sqrt{\Theta^2\left(\frac{\delta\alpha}{\alpha}\right)^2 + \left(\frac{\delta V_s}{\alpha IR_{cold}}\right)^2 + \left(\frac{\delta I}{\alpha I^2 R_{cold}}\right)^2 + \left(\frac{\delta R_{cold}}{\alpha IR_{cold}^2}\right)^2}$$

or in relative terms:

$$\frac{\delta\Theta}{\Theta} = \sqrt{\left(\frac{\delta\alpha}{\alpha}\right)^2 + \frac{\left(\frac{\delta V_s}{V_s}\right)^2 + \left(\frac{\delta I}{I}\right)^2 + \left(\frac{\delta R_{cold}}{R_{cold}}\right)^2}{\left(1 - \frac{R_{cold}}{R_s}\right)^2}}$$

$$R_s = \frac{V_s}{I}$$

where the sensor resistance has been substituted in order to help relate the relative uncertainties. This expression is disturbing, since the uncertainty is very high unless there is a large change in the sensor resistance from the cold resistance. If the sensor resistance is close to the cold resistance, the denominator in the balance of the uncertainty expression can get extremely small. Practice has shown that the resistance ratio can in fact be close to unity, resulting in potentially large foil temperature uncertainties.

Film Coefficient

The film coefficient uncertainty is significantly more difficult to analyze, since the film coefficient is computed using a least-squares linear regression on several uncertain data point pairs. Assuming that runs are made at n currents, resulting in n (Θ_i, q_i) pairs, the film coefficient is calculated from:

$$h = \frac{1}{A_s} \frac{n\sum_{i=1}^{n} \dot{q}_i \Theta_i - \sum_{i=1}^{n} \dot{q}_i \sum_{i=1}^{n} \Theta_i}{n\sum_{i=1}^{n} \Theta_i^2 - \left(\sum_{i=1}^{n} \Theta_i\right)^2}$$

The uncertainty on h is rather complex:

$$\delta h = \sqrt{\sum_{j=1}^{n} \left(\frac{\partial h}{\partial \Theta_j} \delta\Theta_j\right)^2 + \sum_{j=1}^{n} \left(\frac{\partial h}{\partial \dot{q}_j} \delta\dot{q}_j\right)^2}$$

$$\frac{\partial h}{\partial \Theta_j} = \frac{1}{A_s} \frac{n\dot{q}_j - \sum_{i=1}^{n} \dot{q}_i}{n\sum_{i=1}^{n} \Theta_i^2 - \left(\sum_{i=1}^{n} \Theta_i\right)^2}$$

$$- \frac{1}{A_s} \frac{n\sum_{i=1}^{n} \dot{q}_i \Theta_i - \sum_{i=1}^{n} \dot{q}_i \sum_{i=1}^{n} \Theta_i}{\left(n\sum_{i=1}^{n} \Theta_i^2 - \left(\sum_{i=1}^{n} \Theta_i\right)^2\right)^2} \left(2n\Theta_j - 2\sum_{i=1}^{n} \Theta_i\right)$$

$$\frac{\partial h}{\partial \dot{q}_j} = \frac{1}{A_s} \frac{n\Theta_j - \sum_{i=1}^{n} \Theta_i}{n\sum_{i=1}^{n} \Theta_i^2 - \left(\sum_{i=1}^{n} \Theta_i\right)^2}$$

It is important to distinguish between the indices i and j in the partial derivatives, since i is used for complete summations while j points to the data pair corresponding to the jth partial derivative. To take these huge expressions and multiply them by individual uncertainties, and then square them, and then sum them, and finally square root them would be not only tedious but also uninformative. Therefore, a conservative approximation is made by replacing the individual δq_i's and $\delta\Theta_i$'s (uncertainties) with their *maximum* respective uncertainties over all j, the expression becomes:

$$\delta h \leq \sqrt{\left(\delta\Theta_j\right)^2_{MAX} \sum_{j=1}^{n} \left(\frac{\partial h}{\partial \Theta_j}\right)^2 + \left(\delta\dot{q}_j\right)^2_{MAX} \sum_{j=1}^{n} \left(\frac{\partial h}{\partial \dot{q}_j}\right)^2}$$

Of course, this is hardly an overwhelming mathematical simplification, but it does make the math tractable.

Now the partial derivatives must be squared and summed. Invoking the definition of the correlation coefficient, the two partial derivative summations become:

$$\sum_{j=1}^{n} \left(\frac{\partial h}{\partial \Theta_j}\right)^2 = h\frac{n}{r^2} \frac{1}{n\sum_{i=1}^{n} \Theta_i^2 - \left(\sum_{i=1}^{n} \Theta_i\right)^2}$$

$$\sum_{j=1}^{n} \left(\frac{\partial h}{\partial \dot{q}_j}\right)^2 = h\frac{n}{r^2} \frac{1}{n\sum_{i=1}^{n} \dot{q}_i^2 - \left(\sum_{i=1}^{n} \dot{q}_i\right)^2}$$

$$r^2 \equiv \frac{\left(n\sum_{i=1}^{n} \Theta_i\dot{q}_i - \sum_{i=1}^{n} \Theta_i \sum_{i=1}^{n} \dot{q}_i\right)^2}{\left(n\sum_{i=1}^{n} \Theta_i^2 - \left(\sum_{i=1}^{n} \Theta_i\right)^2\right)\left(n\sum_{i=1}^{n} \dot{q}_i^2 - \left(\sum_{i=1}^{n} \dot{q}_i\right)^2\right)}$$

The denominator in each of the partial derivative expressions can be recognized as variances:

$$\sigma_q^2 = \frac{\sum_{i=1}^{n}\left(\dot{q}_i - \bar{\dot{q}}\right)^2}{n-1}, \quad \bar{\dot{q}} = \frac{1}{n}\sum_{i=1}^{n}\dot{q}_i$$

$$so\ \sigma_q^2 = \frac{\sum_{i=1}^{n}\left(\dot{q}_i - \frac{1}{n}\sum_{j=1}^{n}\dot{q}_j\right)^2}{n-1} = \frac{\sum_{i=1}^{n}\left(\dot{q}_i^2 - \frac{2}{n}\dot{q}_i\sum_{j=1}^{n}\dot{q}_j + \frac{1}{n^2}\left(\sum_{j=1}^{n}\dot{q}_j\right)^2\right)}{n-1}$$

$$= \frac{\sum_{i=1}^{n}\dot{q}_i^2 - \frac{1}{n}\left(\sum_{j=1}^{n}\dot{q}_j\right)^2}{n-1} = \frac{n\sum_{i=1}^{n}\dot{q}_i^2 - \left(\sum_{j=1}^{n}\dot{q}_j\right)^2}{n(n-1)}$$

$$similarly\ \sigma_\Theta^2 = \frac{n\sum_{i=1}^{n}\Theta_i^2 - \left(\sum_{j=1}^{n}\Theta_j\right)^2}{n(n-1)}$$

Finally, the film coefficient uncertainty is estimated by:

$$\frac{\delta h}{h} = \frac{1}{r\sqrt{n-1}}\sqrt{\left(\frac{\delta\Theta_{MAX}}{\sigma_\Theta}\right)^2 + \left(\frac{\delta q_{MAX}}{\sigma_q}\right)^2}$$

This is a very important uncertainty relation, but it must be interpreted properly. First, as expected, the uncertainty is lowest for a perfect linear curve fit, or r close to unity. In actual experiments, this is achieved as r^2 is typically on the order of 0.995 or higher. The uncertainty relation also points out the familiar trend that the uncertainty goes down with the square root of the number of points used in the regression, or equivalently the number of currents used during the data acquisition.

The final thing to note is that the relative uncertainty contributions of the heat transfers and sensor temperatures is scaled not on some mean value, but rather on the variance of the data used for the regression. These variances are <u>not</u> the same as the variance on a given value at one current (i.e., the root-mean-square noise fluctuations on the signals, which are desired to be small); instead, these variances are a measure of the spread of currents run. The uncertainty is lowest when these variances are *highest*. This expression simply states that the slope of the q-Θ line is easier to determine accurately when a wide *range* of q's and Θ's are used. This is equivalent to running as large a range of currents as possible. The highest current set is determined by the burnout current of the sensors or the maximum voltage potential of the current source. The lowest current is zero, but at very low currents the basic quantity uncertainties become huge.

Wall Shear

The final uncertainty relation is for the calculation of the wall shear. The wall shear is given by:

$$\tau_w \propto h^3$$

so the shear uncertainty is trivially

$$\frac{\delta\tau_w}{\tau_w} = 3\frac{\delta h}{h}$$

It is important to note that the calibration uncertainties are not included here. This analysis is for determining the relative uncertainties between measurements made by one sensor at different locations of the model in different flow conditions. This relative uncertainty determines the precision with which one can determine the location of flow separation, which is the most important piece of information sought after. The uncertainty due to the calibration is huge, on the order of 25%, and is a bias uncertainty, not a random one. This uncertainty, while much larger, is also secondary in importance due to the fact that it does not inhibit one from determining the location of separation.

Non-Ideal Sensor Operation Uncertainties

There are several other sources of uncertainty that result from non-ideal operation of the sensor system. The most significant is current leakage into the differential amplifiers. If the resistors that set the amplifier gain are not set high enough, a small but important amount of current can leak into the amplifiers. The current source used is a sinking current source, so the desired current is accurately set at the exit lead of the last sensor in a chain of sensors. At each input to each differential amplifier, as high as several tenths of a milliamp of current can leak into the differential amplifier. While this is much smaller than the 0.1 mA resolution of the DAC setting the current sources, the effect is summed to each previous sensor in the chain. Therefore, the first sensor will have the highest current of all of the sensors, and the difference can easily be several milliamps. More importantly, this uncertainty quickly becomes amplified, as that current error results in a heat transfer error and sensor temperature error, which results in an even larger film coefficient error and a yet larger wall shear error. This can be corrected for by simply analyzing the differential amplifier circuit and computing the current leakage, and thus the true sensor current, for each sensor. However, this results in more necessary measurements, uncertainty analyses, and computation complexity and expense, so current leakage is avoided as much as possible by using megohm-sized resistors for all differential amplifiers. However, if the resistors are too large, the natural input bias current of the op-amps passing through the resistors will result in a huge no-load voltage offset. The resistors used in these test, $R1 = 100$ kΩ and $R2 = 1.0$ MΩ adequately minimize current leakage effects below the resolution of the hardware while keeping post-amplified voltage offsets on the order of millivolts.

Anemometer Hardware

Anemometer Operation: Overview

The anemometer boards operate in a constant current mode. The host PC sends a DC voltage via the D/A line on the HSDAS-16 to a voltage-controlled current source. This current source supplies each *string* of sensors with a constant current. The voltage across each sensor is measured with a differential amplifier. Then these voltages are fed through two levels of multiplexers to reduce the 1024 sensor voltages to 4 multiplexer voltages. The multiplexers are driven by eight counters from a CTRTM-10 counter board installed in the host PC. The supplied data acquisition software performs all hardware synchronization and data bookkeeping.

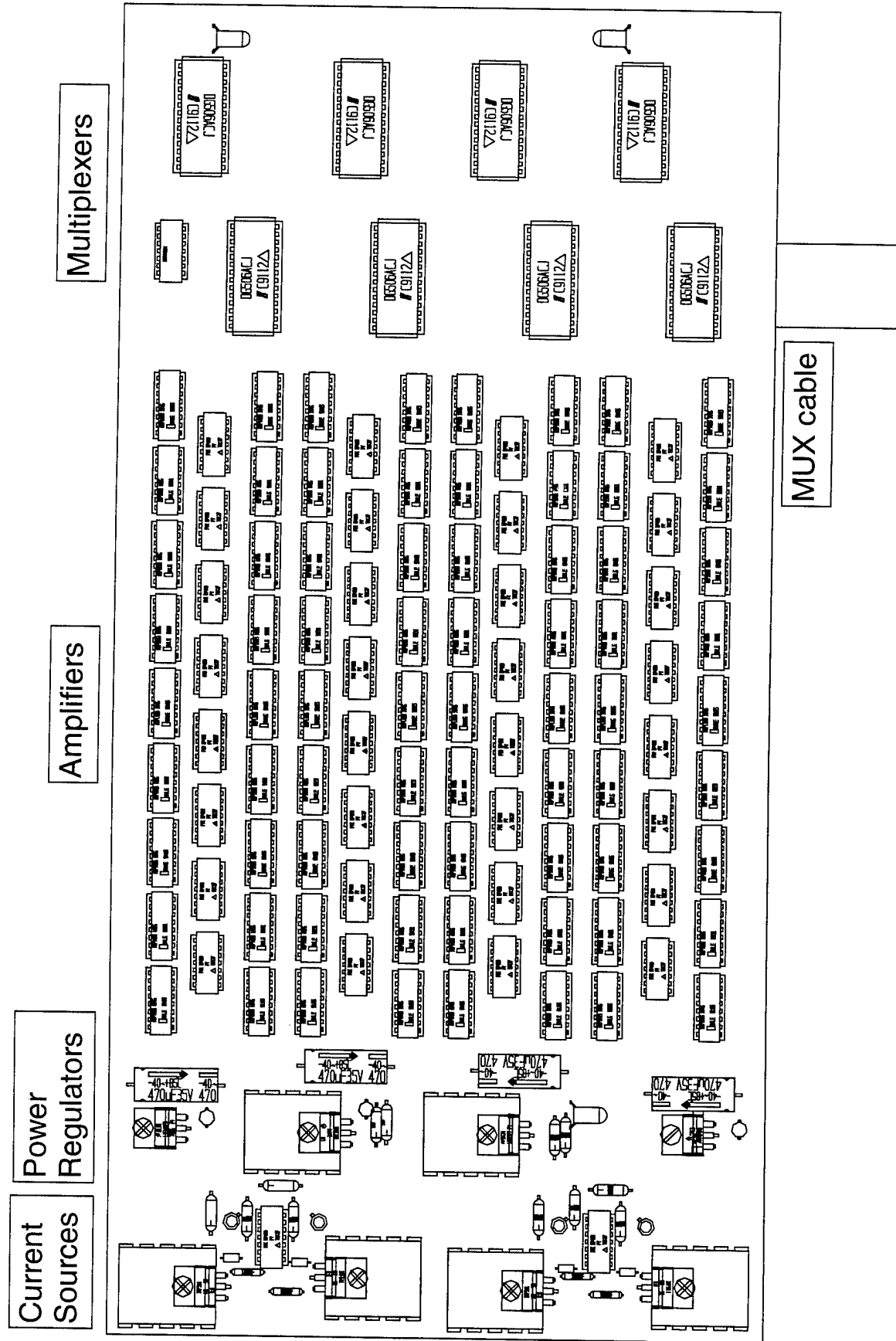The physical board layout is shown in Figure 3 and the cable layout is shown in Figure 4.

Current
Sources

Power
Regulators

Amplifiers

Multiplexers

MUX cable
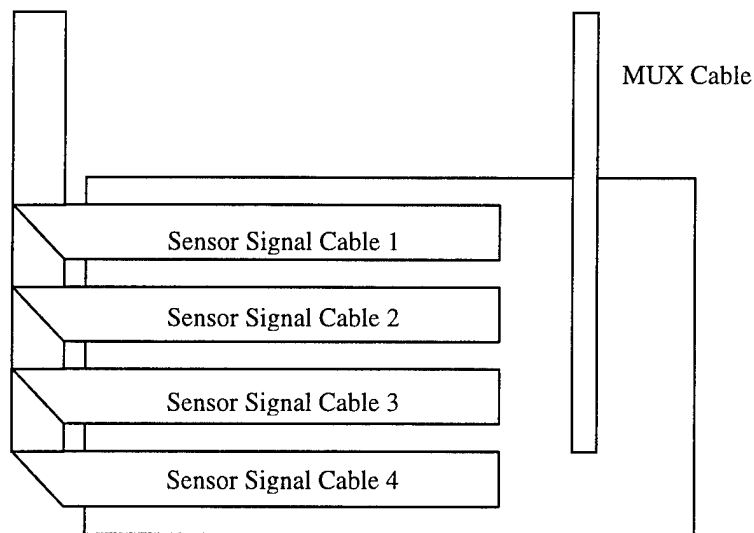
Figure 3. Board component layout.

Figure 4. Back of anemometer boards.

Power Supplies

The Main Power Supply contains three regulated DC power supplies. These supplies are connected to a 120 VAC outlet. The Main Power Supply provides +28V, -28V, and +12V DC power rated at 18A, 18A, and 3A respectively. The +/-28V power supplies are manufactured by Todd, Inc. and the +12V power supply is manufactured by Sola, Inc. The +/-28V power feeds are used for +/-20V supplies which powers most of the components on the boards, including the current sources which draw a lot of power. The +12V power supply is used to eventually generate 5V power for some very-low-power logic chips. The power is delivered over the majority of the rotating arm length by a four conductor, #14 AWG power cable. The pinouts for the Amphenol 20-4 connector are given below in Figure 5.
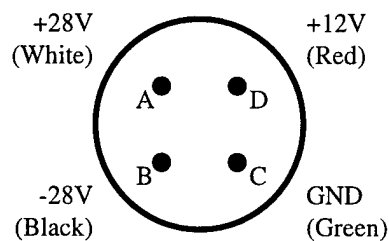

Figure 5. Main Power Cable and Connectors.

Before going down the sting assembly to the model the power is redistributed into the ribbon cables. Essentially, 15 conductors are used for each of the +28V, -28V, and +12V power lines. Two conductors are used for the low power +12V power lines. See the section on the Master Multiplexer for detailed ribbon cable pinouts.

19

The power is brought into the anemometer box at which point it is made available to the individual boards by a power distribution block. This block basically consists of 8 power connectors fastened together. The pinout for the power connectors is given below in Figure 6.
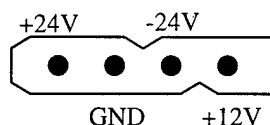

Figure 6. Power Connectors.

The power is further regulated and stepped down by voltage regulator circuits on the anemometer boards. The +28V power is regulated down to +20V. The -28V power is regulated down to -20V. The +12V power is regulated down to +5V. The amplifiers, current sources, and multiplexers are all powered by +/-20V. Only the hex inverters require +5V power supplies.

Current Sources

The current sources work by providing +20V power at the "top" of the sensor string (sensor 32), and floating the "bottom" of the sensor string between +20V and -20V to set the current appropriately. The current passes through a resistor in the current source which converts the current to a voltage. This voltage is fed through an amplifier circuit as a means of feedback for the current source. This amplifier circuit regulates an IRF511 power MOSFET, which supplies the current.

The current sources can be calibrated against the control voltage and can be very linear, but they tend to drift when they get hot. Therefore, the current output is measured directly by replacing sensor 32 with a very high precision resistor (2.500+/-0.05% Ω). This provides a very accurate method for current measurement. Therefore, it is important to keep in mind that each string has 32 "sensors", but in fact each string is wired to *31* hot film sensors and 1 current-monitoring high precision resistor.

Differential Amplifiers

Since the "top" of the sensor string is typically at a 20V potential and the "bottom" is anywhere from +20V to -20V, and since the HSDAS-16 has a voltage input range of +/-10V, the voltages from individual sensor leads can not be fed directly into the data acquisition board. Therefore, differential amplifiers are used to amplify the voltage across each sensor, and this voltage, Vs_i, is digitized by the HSDAS-16. This configuration provides the added benefit of amplifying the differential voltage across the sensor before analog-to-digital conversion, thus maximizing AD resolution.

A representative amplifier circuit Is show below in Figure 7. The current flows through the sensor resistance, Rs_i, and any lead resistance $Rlead_i$. The voltage generated across this sensor, Vs_i, is seen at the inputs to the differential amplifier. The voltage at the output of the amplifier is 10 times the voltage potential across the

sensor. A voltage divider, discussed in detail in the section *Master Multiplexer,* reduced the effective nominal gain to 5.
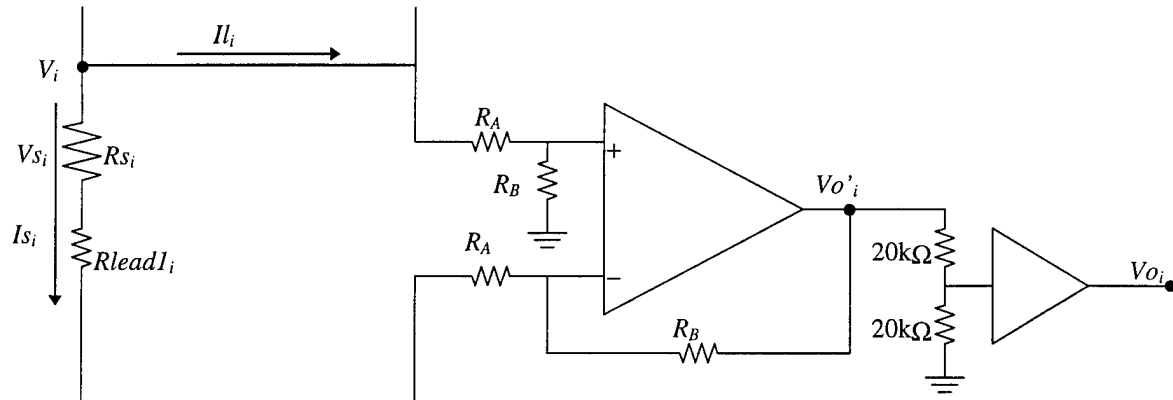

Figure 7. Typical differential amplifier. Multiplexers are not shown for simplicity.

There are several non-idealities that complicate the usage of the board. The first is that the amplifiers do not have a perfect gain of 5.000. The second is that the amplifiers tend to have finite output offsets, and there is no provision for adjusting out such an offset voltage. Therefore, each of the 1024 amplifiers must be individually calibrated for gains and offsets.

The more important non-ideality is due to the fact that the amplifier circuit does not have an infinite input impedance. Small but significant leakage currents flow through the gain-setting resistors in the amplifier circuit to the ground and output potentials. When an entire string is examined as a system, this current leakage problem is cumulative; that is, the sensor nearest the "top" of the string, sensor 32, may only experience a current leakage of a few tenths of a milliamp. However, several sensors further down the string the true sensor current will be smaller by the tenths-of-a-milliamp for each sensor previous, or on the order of several milliamps. Therefore, the current tends to be highest in sensor 32 and lowest in sensor 1 by a very significant amount. This effect can and must be accounted for in all calibrations and data reductions (see Current Leakage Corrections).

Multiplexer Circuits

Harris DG506ACJ 16 channel multiplexers are used to reduce the 1024 sensor voltages down to 4. There are 8 multiplexers on each board. Since each multiplexer can receive 16 inputs, there are 2 multiplexers per string. Each multiplexer requires 4 digital lines to select the appropriate address. These digital lines are first brought through a 74HC04 hex inverter. This hex inverter guarantees that the digital levels going to the multiplexers are clean and non-attenuated.

Master Multiplexer (9th Board)

The eight boards are connected together by the Master Multiplexer which sends the current source control voltage and digital multiplexer address lines to each board and receives the eight analog outputs corresponding to the eight multiplexers per board. These signals are transmitted through the MUX cables, as indicated above in Figure 4.

The MUX cables are 17 conductor ribbon cable. These cables interface with the Master MUX board through 20 pin headers and IDC connectors. The pinouts for these connectors are given below in Figure 8.

White	MUX 6	2	· ·	1	MUX 8	Purple
Orange	MUX 2	4	· ·	3	MUX 4	Brown
Green	A2 on Muxes	6	· ·	5	Current	Red
Purple	A0 on Muxes	8	· ·	7	A1 on Muxes	Blue
Brown	GND	10	· ·	9	A3 on Muxes	Gray
	NC	12	· ·	11	NC	
Red	MUX 3	14	· ·	13	MUX 1	Yellow
Black	MUX 5	16	· ·	15	GND	Orange
	NC	18	· ·	17	MUX 7	Gray
	NC	20	· ·	19	NC	

Figure 8. MUX cable headers, looking a t *back* of Multiplexer Board. Abbreviations same as above figure.

The current source requires a *negative* control voltage. Therefore, the positive computer digital-to-analog voltage command signal is fed through an inverting amplifier (Figure 9) on the Master MUX board before being transmitted to the individual anemometer boards. This amplifier is configured to attenuate the control voltage. A pot is used to adjust this gain which effectively allows the user to set the full range of the current sources. For the 1995 tests, this pot was set so that a +10V command gave roughly a 340 mA output on the current sources. This gain was chosen so that the user could not inadvertently set the current sources at a high enough current to burn out the sensors in air.
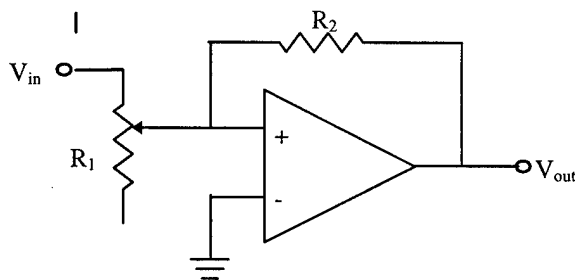
Figure 9. Current source control inverting amplifier circuit. R_1=200 kΩ pot, R_2=8.26 kΩ. V_{out}=-(R_2/R_1)V_{in}.

Eight digital lines are brought into the board from the host PC to set the multiplexer addresses. The first four digital channels (MSB's) on the Master MUX set the multiplexers on the Master MUX board. They are fed through a MM74C14N Schmitt Trigger and a MM74HC04N Hex Inverter before going to the on-board multiplexers.

The remaining four digital lines (LSB's) are fed through a Schmitt Trigger and then disseminated to the anemometer boards via the header shown in Figure 10.

GND	2	· ·	1	+24V	
Current	4	· ·	3	-24V	
AOUT2 Hi	6	· ·	5	AOUT1 Hi	
AOUT4 Hi	8	· ·	7	AOUT3 Hi	
AOUT2 Lo	10	· ·	9	AOUT1 Lo	
AOUT4 Lo	12	· ·	11	AOUT3 Lo	
D2	14	· ·	13	D1	
D4	16	· ·	15	D3	
D6	18	· ·	17	D5	
D8	20	· ·	19	D7	

Figure 10. Input Header on Multiplexer Board.

Since each multiplexer receives 16 inputs and each anemometer board has eight analog outputs, each multiplexer on the Master MUX services two boards; therefore, there are 4 multiplexers on the Master MUX board. The first multiplexer, which is connected to AD channel 1 on the HSDAS board, is wired to boards 1 and 2. Multiplexer 2 is wired to boards 3 and 4; etc. The main connector coming from the data acquisition computer and going to the Master MUX is shown in Figure 11.

AOUT1 Hi	1	• •	2	AOUT2 Hi	+24V	1	• •	2	+24V
AOUT3 Hi	3	• •	4	AOUT4 Hi	+24V	3	• •	4	+24V
AOUT1 Lo	5	• •	6	AOUT2 Lo	+24V	5	• •	6	+24V
AOUT3 Lo	7	• •	8	AOUT4 Lo	+24V	7	• •	8	+24V
D1	9	• •	10	D2	+24V	9	• •	10	+24V
D3	11	• •	12	D4	+24V	11	• •	12	+24V
D5	13	• •	14	D6	+24V	13	• •	14	+24V
D7	15	• •	16	D8	+24V	15	• •	16	-24V
Current	17	• •	18	+24V	-24V	17	• •	18	-24V
-24V	19	• •	20	GND	-24V	19	• •	20	-24V
GND	21	• •	22	GND	-24V	21	• •	22	-24V
GND	23	• •	24	GND	-24V	23	• •	24	-24V
GND	25	• •	26	GND	-24V	25	• •	26	-24V
GND	27	• •	28	GND	-24V	27	• •	28	-24V
GND	29	• •	30	GND	-24V	29	• •	30	-24V
GND	31	• •	32	GND	+12V	31	• •	32	+12V
GND	33	• •	34	GND	GND	33	• •	34	GND

Figure 11. Main Cable entering anemometer box and going to Master MUX.

The multiplexer outputs are then fed through a 50% attenuation voltage divider (see Figure 12). The output of this divider is fed through a LM6321N High Speed Buffer, and the buffer output is connected in series with a 50Ω resistor, which in turn is hooked up to the output ribbon cable lines. The end of the cable at the computer is terminated to ground with a potentiometer which is nominally 50Ω. 50Ω impedance cable was not used as the long-distance transmitting medium. Instead, higher impedance ribbon cable was used. Therefore, this pot can be used to better match the transmission impedances. The cable is short enough, and data acquisition speeds slow enough, to prevent signal transmission from being a problem.
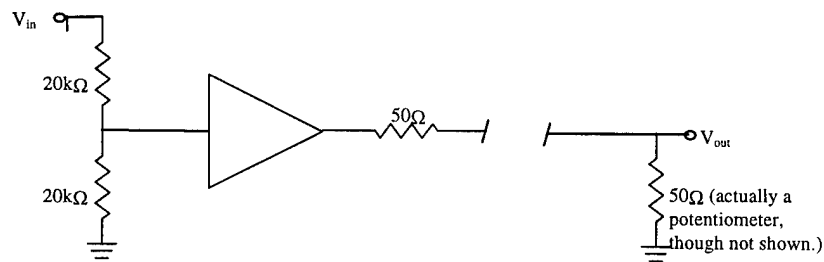

Figure 12. Buffers. Note 50% attenuation due to voltage divider.

Data Acquisition Hardware and Operation

The host PC contains an Analogic HSDAS-16 data acquisition card and an Analogic CTRTM-10 counter/timer card. The HSDAS-16 is a 16 channel, 16-bit A/D board with 2 12-bit D/A channels. One D/A channel is used to control the current sources. Four A/D lines are used in differential mode to sample the sensor voltages. The data acquisition is software triggered, but is paced externally by the counter timer card.

Nine of the ten counter-timer channels on the CTRTM-10 board are used to run the data acquisition system. The first channel is a 15.625 kHz square wave that is used as a pacing signal for the A/D board. Each of the eight subsequent timer channels used are half of the frequency of the previous channel. Thus, the frequencies of the nine timer channels used are:

Counter	Description	MUX input	Frequency
1	AD pacing	na	15625
2	D2*	A3	7812.5
3	D3*	A2	3906.25
4	D4*	A1	1953.13
5	D5*	A0	976.56
6	D6**	A3	488.28
7	D7**	A2	244.14
8	D8**	A1	122.07
9	D9**	A0	61.04
10	NC	na	na

Figure 13.Output of CTRTM-10. (*To anemometers;**To Master Multiplexer)

These signals are switched in phase. Also, it is important to remember that these signals are inverted prior to addressing the multiplexers.

To locate the sensor corresponding to a given timer output vector, the following algorithms are used. In these equations, Dn refers to the nth digital channel, as given in the table above. The A/D channel number is referred to by the symbol A.

$$\text{board number } (1 \text{ thru } 8) = 2 * A - D2$$
$$\text{string number } (1 \text{ thru } 4) = 2 * D3 + D4$$
$$\text{sensor number } (1 \text{ thru } 32) = 16 * D5 + 8 * D6 + 4 * D7 + 2 * D8 + D9$$

The data is acquired via Direct Memory Access (DMA). The data, when acquired, is interleaved; that is, the data is in one long linear record that must be appropriately sorted. The following algorithm is used to determine the record number given a known board, string, and sensor number triplet.

Current Leakage Corrections

Corrections were made in both the amplifier calibrations and in the data reduction for the leakage of current from the sensors through the amplifiers. This meant that despite the efforts of the constant current sources, the currents were slightly, but predictably, different for each sensor. The algorithm proceeded as follows, using the nomenclature shown in Figure 14. Using the measured voltage and the known gains and offsets for each sensor amplifier, the actual sensor voltages were computed from:

$$Vs_i = (Vo_i - O_i) / G_i \text{ for i = 1 to 32}$$

Following this, the lead voltages for each sensor were computed. The sensor at the end of the string was the +20V supply voltage. This was measured for each board as accurately as possible as it varied from +20V by as much as 1%. Then the lead voltages were computed in succession, thus:

$$V_{32} = V_{in}$$
$$V_i = V_{i+1} - Vs_{i+1} \text{ for i = 31 to 1}$$

Next, the leakage currents through each lead were computed as simply the current through the amplifier resistances considering the lead voltage drops, thus:.

$$Il_{32} = \frac{V_{32}}{R_A + R_B}$$

$$Il_i = 2\frac{V_i - Vo_{i+1}}{R_A + R_B} \text{ for i = 31 to 1}$$

And finally, the sensor currents were computed by first computing the current through the fixed resistor, accounting for lead resistances to and from that resistor, and then the currents were successively summed with the leakage currents to determine each sensor current:

$$Is_{32} = \frac{Vs_{32}}{R_{cal} + R_{lead1} + R_{lead2}}$$
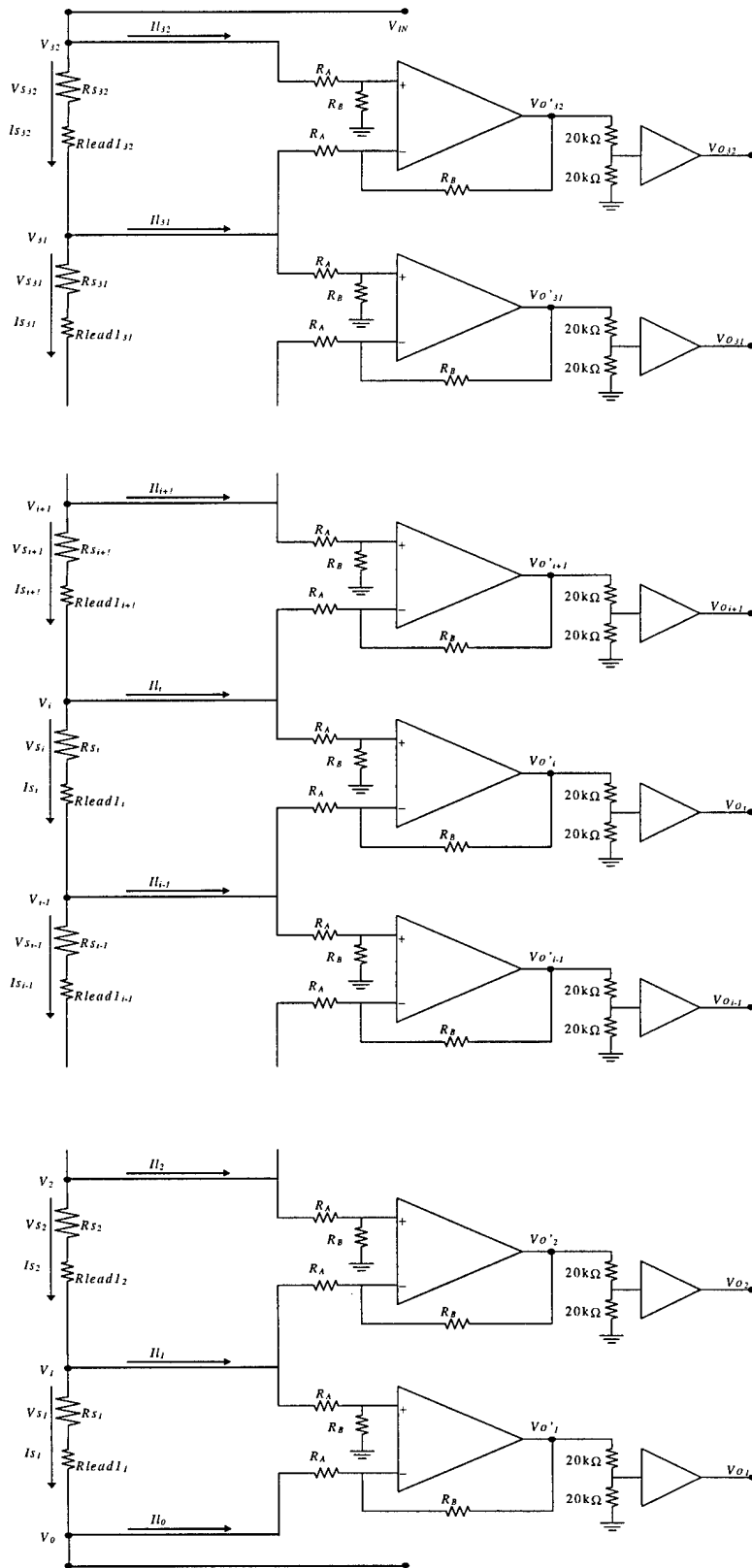
$$Is_i = Is_{i+1} - Il_i$$

Figure 14. Anemometer system and current leakage calculation nomecalture.

Amplifier Calibrations

Each of the 1024 amplifiers was calibrated by connecting a string of 31 very high precision (+/-0.05%) 2.500Ω resistors to individual amplifier strings. Using various current settings, and using an HP 3478A precision digital multimeter to measure both input current and voltage (at node 32), and implementing the current leakage correction scheme discussed above, a least squares fit was used to determine a gain and offset for each amplifier. As an approximation, since the gain and offset are used in the current leakage calculations, a nominal gain and zero offset were used for the current leakage corrections in this case. The amplifier characteristics were then stored in the file hf_cal.dat.

Software

Below is a very brief description of the software developed for these tests. This software is remains on the host computer used for this project, and is additionally available on diskette.

Library Header: hf_lib.h

This head file contains declarations for all functions in the library source file. It also declares several structures used to organize the data. The structures in this implementation are only multi-dimensional arrays. However, by using the structure construction, it allows entire blocks of data to be allocated or passed very easily and it makes accessing specific strings, boards, sensors, etc. less ambiguous in the various programs.

General Library Routines: hf_lib.c

The following routines listed represent the main code modules used to run the anemometer boards, collect the data, and output the data. Each routine is listed thus:

Routine	Description
setup_HSDAS	Initializes HSDAS-16 board and prepares it for data acquisition
setup_CTRMR	initializes timer board and sets all digital outputs to LOW
shutdown_HSDAS	disables HSDAS card
shutdown_CTRMR	disables timer card
set_current	sets the current source to the desired current via the D/A line on the HSDAS card
error_check	generic error checking routine; if value passed to it is negative, there is an error, at which point the message is output and the program is terminated
get_hf_data	acquires voltages from all sensors and places the data in just a huge 1-dimensional array
arm_timer	starts the timer
disarm_timer	stops the timer
my_delay	generic time-delay routine
set_high	sets the specified timer output to HIGH (used for selecting individual sensors instead of sequencing through all sensors)
set_low	sets the specified timer output to LO (used for selecting individual sensors instead of sequencing through all sensors)
parse_data	takes the huge 1-dimensional array of data from the get_hf_data routine and sorts it into a hot_film structure, which means the data from a given sensor on a given string on a given board can be selected very easily
select_sensor	sets the MUXES so that the indicated sensor is selected, allowing the user to measure the response on just one sensor for applications such as time response (the user still needs to select the appropriate A/D line to read the desired sensor.
time_response	measures the step-time response of a given sensor to gage its frequency response
output_hf_data	outputs all sensors data to the screen in text mode

output_hf_graphics	outputs all sensors data to the screen in graphics mode, which allows all voltages to be on the screen simultaneously
get_Rlead	reads in the lead resistance data from the hf_rlead1.dat file

Testing Software: hf_test.c

This program was used more than any other during the course of the project. It allows the user to set the current sources to any desired achievable current and then displays *all* 1024 sensor voltages on the screen, organized as visible boards with 4 strings on each board. This program was used extensively to test the system.

Amplifier Calibration: hf_cal.c and hf_c_cmp.c

These are the programs that were used to calibrate all 1024 amplifiers. A special calibration block with 31 very high precision resistors was plugged into each string one at a time. A multimeter was used to monitor the exact supply current and voltage entering the resistor string. The program would cycle the resistors through several currents and use the resultant voltages, along with the full current leakage corrections, to compute the gains and offsets on each amplifier.

Data Acquisition: hf_dac.c

This was the program used to acquire the data for the actual test runs. It reads in a file which tells it how many currents it will run and what the value of those currents are, and then quickly cycles through each of those currents at user initiation and reads in voltages from each sensor. Then this program parses the data (organizes it according to which board and string each voltage came from) and outputs it to a file named on the command line.

Data Reduction: hf_red.c

This program reads in the raw data from hf_dac.c and reduces it according to the algorithms listed earlier in this document.

Chronological Overview of Experiences

Hardware Preparation

Electronics

The original hardware was in a semi-completed state when the current project was initiated. The eight anemometer boards were mostly fabricated, but each board needed to be fitted with interfacial connectors for signal inputs, outputs, and power delivery. Ribbon connectors were placed on both the control signal lines that command the current sources and multiplexers, and the sensor lines, that deliver the sensor currents and voltages from the anemometer boards to the sensors and back. Also, a four-pin connector was installed with power lines to deliver +28V, -28V, +12V, and GND power lines to the boards. The pinouts for these connections are described in detail in sections that follow. All eight boards were tested thoroughly and bad components were replaced. In addition, the 32nd channel of each sensor string was hard-wired with a very high precision (0.05%) 2.5Ω resistor as a direct measurement of the sensor string current.

After these modifications were completed, the ninth "Master Multiplexer" board needed to be completed. This board had the bare components originally laid out, but required extensive modification. Connectors were installed on the board to accept the command lines from the anemometer boards, and these connectors were wired appropriately into the multiplexers and power circuits. Connectors were also installed to interface with the computer and power supply cables. Details of these connectors are also described below.

A 200 ft. long cable was constructed to deliver up to 20 A to the anemometer electronics at over 40 volts potential, or over 800 W of power. Mercury Wire was contracted to construct custom cable assemblies that featured: 34 conductors, each #28 AWG; waterproof insulation and jacketing; waterblocking in between the individual conductors to prevent taking on water via capillary action; and sealed ends to prevent water entry into the construction. These water proof cables were used in all water-borne cable applications, including going from the anemometer housing to the individual sensors, and going from the anemometer housing to the main computer/power supply cable. To act as a power supply cable, 15 of the #28 AWG conductors (from two cable assemblies) were wired in series for each of the 3 major power lines (+28V, -28V, GND).

Computer Hardware and Software

An AST 486-25SX PC was purchased to perform the data acquisition and reduction. It was fitted with an Analogic HSDAS-16 data acquisition card and an Analogic CTRMR-10 timer card. The timer card produced the eight mutliplexer channel counters and one data acquisition timing channel to allow the sensors to be selected and sampled very quickly (15625 Hz, or 0.066s to read a single voltage from each of the 1024 sensors). The data acquisition card provided 4 (of a possible 16) channels of 16-bit resolution for sampling the sensor voltages. It also provided a digital-to-analog voltage line to control the current sources on the anemometer boards.

Various programs were written for general maintenance and data acquisition. All codes were written in Borland C v3.1. Some of the codes used a graphics library for SVGA graphics. Codes were written to allow a user to power up the current sources and inspect the voltages on all sensors; calibrate the amplifiers on all boards; make frequency response measurements on individual sensors; take data from all sensors during actual runs; and reduce that data. All codes were implemented using a separately-written library of routines that make future code development simple without needing to deal with detailed, low-level hardware issues. These routines are described in detail below.

Anemometer Housing

The original box designed from this system was only partially completed. It involved "U" shaped Plexiglas ends of different sizes, forming a semi-conical shape; a Plexiglas lower shell; and a sheet rubber bladder surrounding the entire outside of the box. The "U" shape was necessary because the box was to be installed in the tail of the model and needed to straddle the sting. The conical shape was necessary to maximize the usage of space inside the converging model tail. The original box was designed with the bladder in order to equalize the pressure difference between the inside and outside of the box at submerged depths of 20' so as to unload all of the Plexiglas portions of the box. It was intended to fill the box with SylGuard gel for improved cooling and to impede waterproofing failure. All wires were to be permanently glued in holes in the Plexiglas box front, and permanently wired to the anemometer boards.

For many reasons, this box was quickly scrapped. First, all of the Plexiglas pieces had cracked with age. Also, it was clearly specified that the electronics needed to be removable, and thus required connectors to interface all of the wires to the box. Finally, there was little faith in the bladder's ability to provide a water-tight seal. Therefore, a new box was designed and manufactured.

One of the first steps that preceded box design was the design of the connector system for bringing 32 cables with 34 conductors each into the box from the sensors, and to provided for two of the same to leave the box to go to the computer. This is very challenging, since the small box provided very little frontal area for over 1000 conductors or for the amount of space that connectors for such a number of connectors would take up. To solve this problem, the cable assemblies were fitted with standard 34-pin ribbon connectors (see Figure 15a), and the cables were rolled to orient the connector parallel (instead of perpendicular, as is usually the case) with the cable (Figure 15b). This provided a high density of pins versus frontal area, as all 34 pins now required barely twice the cross sectional area of the bare cable itself. Then, standard PVC unions were used to bring bundles of eight such cable assemblies into the box (Figure 16). Four of these unions, two on each side of the box, provided enough room to bring in all of the cables, and sealed off the box with O-rings installed in the unions. The cables were then individually connected to the boards via the ribbon cables. Figure 17 shows a diagram of the anemometer housing.
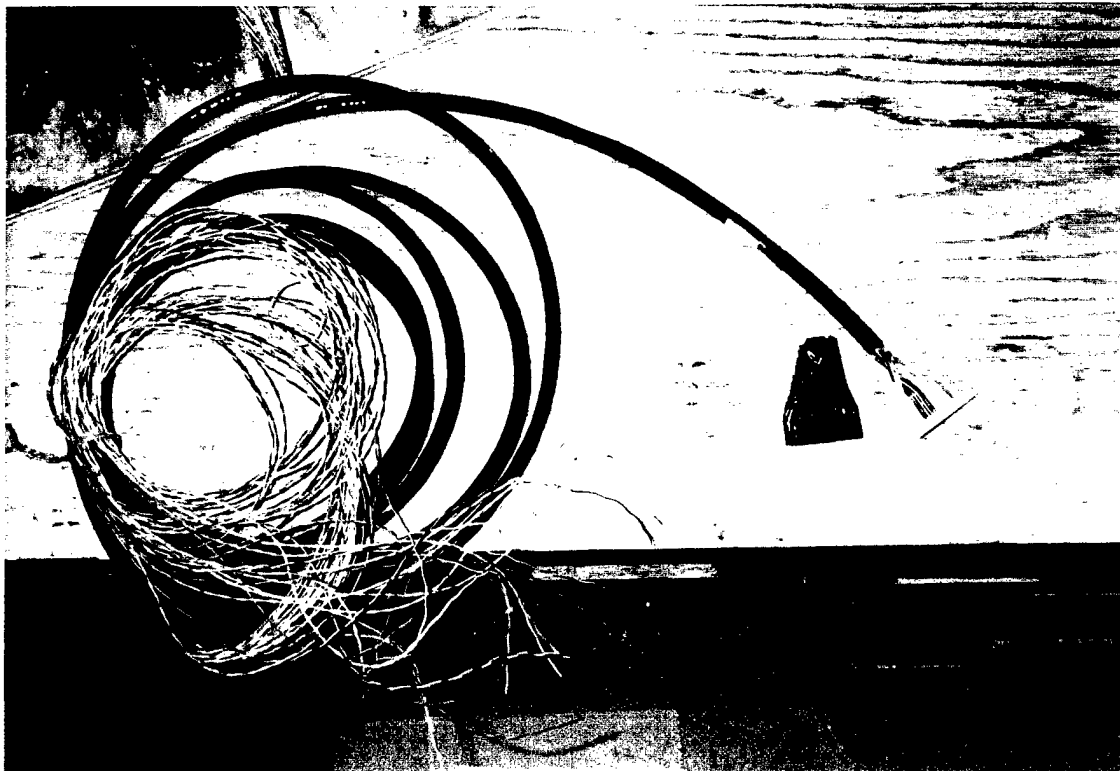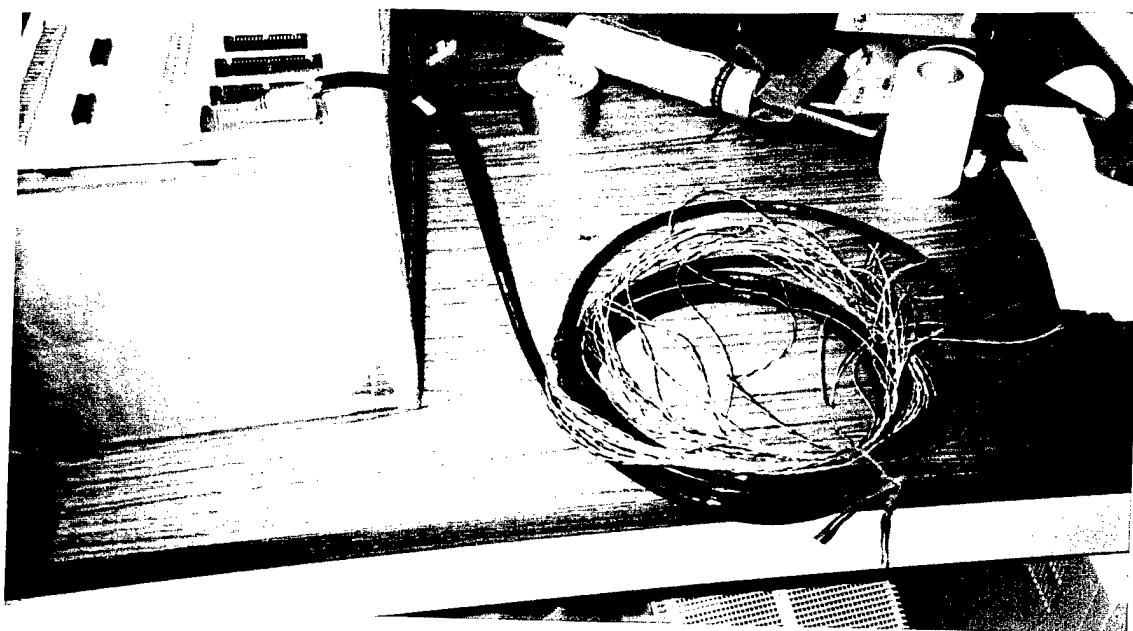
Figure 15a. Water-proof cables before rolling.

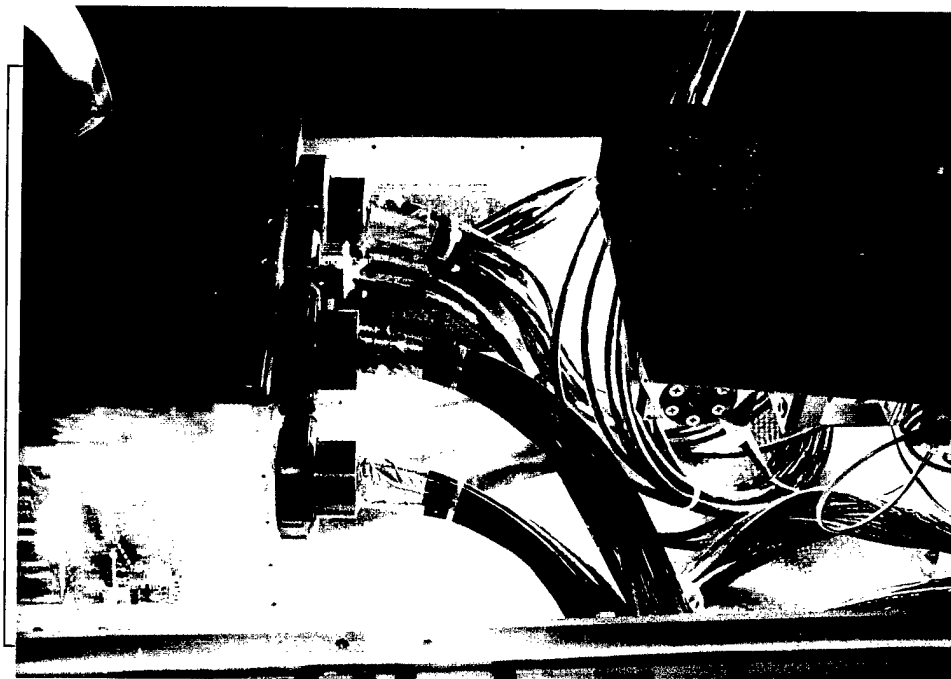Figure 15b. Water-proof cables rolled.

Figure 16. Cables entering box through PVC unions.

Stern   Bow

19.500

.677

10.328

7.875

7.000

13.400

ANEMOMETER HOUSING
Basic Final Configuration
Todd G. Wetzel
8/15/94

16.5" diameter circle represents
the INNER diameter of the model at 180°
that I took off the drawings you faxed me.
This is snug, but should work if my
16.5" diameter measurement is accurate.

Cables exit box from
connectors at these ports. Connectors
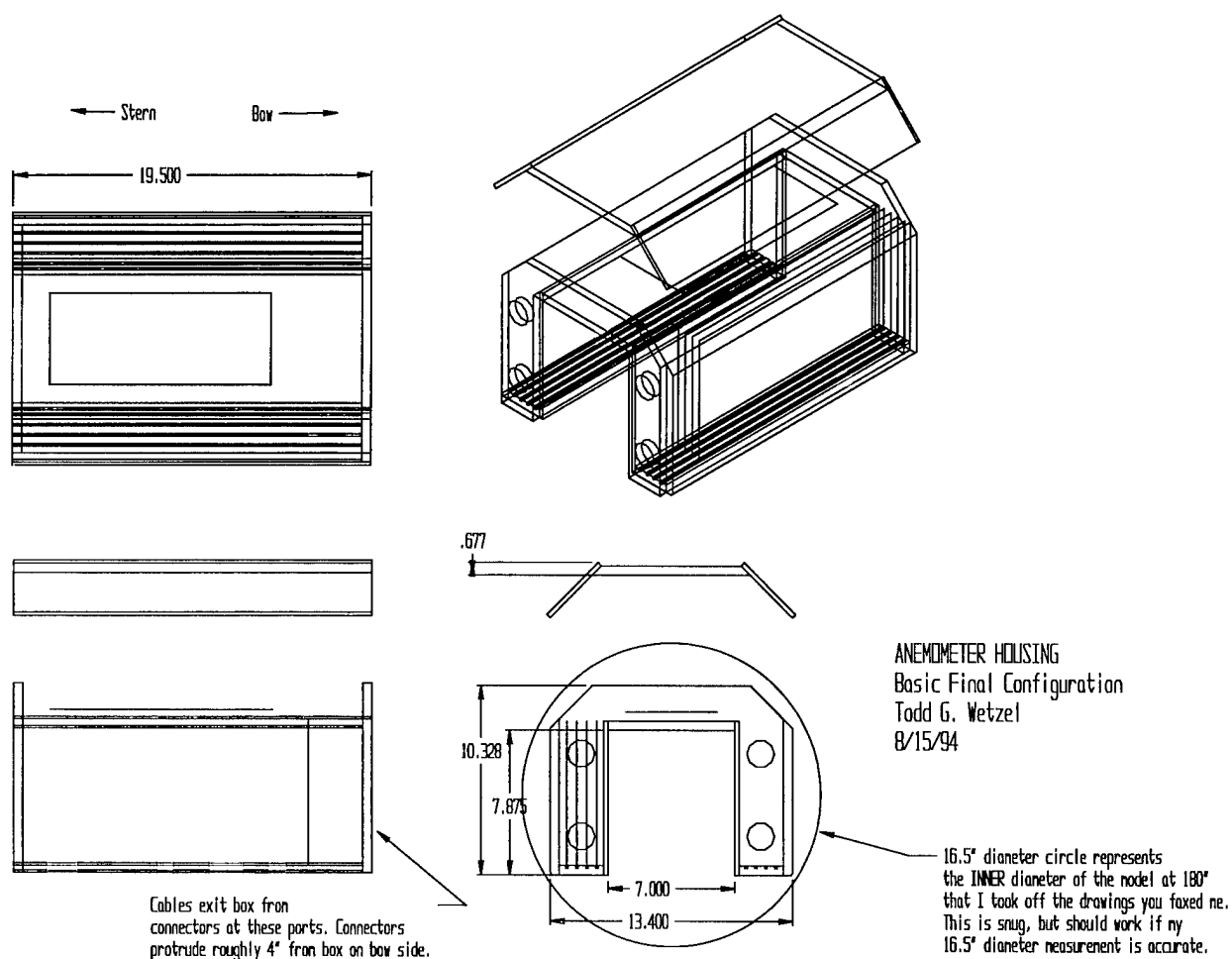protrude roughly 4" from box on bow side.

Figure 17. Anemometer housing construction.

Model Instrumentation

Sensors were installed in 14 rings on the model spaced 5° apart. No sensors were placed on the seams between the top and bottom model halves, so there were 70 sensors in a ring, for 980 total sensors used. Since each string (a "string" being a grouping of sensors hooked up to the same current source) includes only 31 sensors, some strings were split between two rings. Because of this, a detailed sensor map was required to relate sensors described in board-level "coordinates" (that is, in terms of board number, string number, and sensor number) to sensors described in model "coordinates" (ring number, circumferential location). A sensor map is provided in Figure 18. The sensors are numbered in terms of a string number and a sensor number, separated by a dot. The strings number from 1 to 32. Strings 1 through 4 originate from board 1; strings 5 through 8 originate from board 2; etc. up through board 8. The software implementation of the sensor mapping is described in the software section below.

Sensor Map

32.30 to 32.31 unused

24.29 to 24.31 unused

21.14 to 21.31
22.1 to 21.20
21.16 to 21.1
20.31 to 20.13
19.9 to 19.31
20.1 to 20.12
19.8 to 19.1
18.31 to 18.5
17.1 to 17.31
18.1 to 18.4

23.25 to 23.31
24.1 to 24.28
23.24 to 23.1
22.31 to 22.21

25.1 to 25.31
26.1 to 26.4
27.8 to 27.1
26.31 to 26.5
27.9 to 27.31
28.1 to 28.12

29.16 to 29.1
28.31 to 28.13
29.17 to 29.31
30.1 to 30.20
31.24 to 31.1
30.31 to 30.21
31.25 to 31.31
32.1 to 32.29

1.1 to 1.31
2.1 to 2.4
3.8 to 3.1
2.31 to 2.5
3.9 to 3.31
4.1 to 4.12

5.16 to 5.1
4.31 to 4.13
5.17 to 5.31
6.1 to 6.20
7.24 to 7.1
6.31 to 6.21
7.25 to 7.31
8.1 to 8.28

10.1
9.31 to 9.1
8.31 to 8.29
10.2 to 10.31
11.1 to 11.5
12.9 to 12.1
11.31 to 11.6

12.10 to 12.31
13.1 to 13.13
14.17 to 14.1
13.31 to 13.14
14.18 to 14.31
15.1 to 15.21
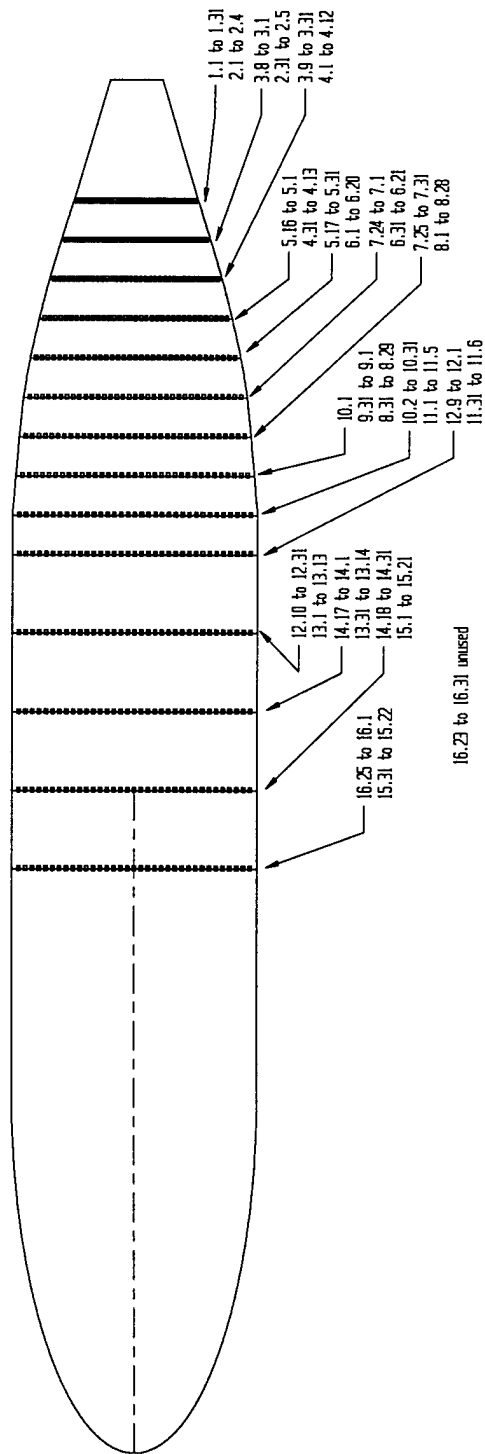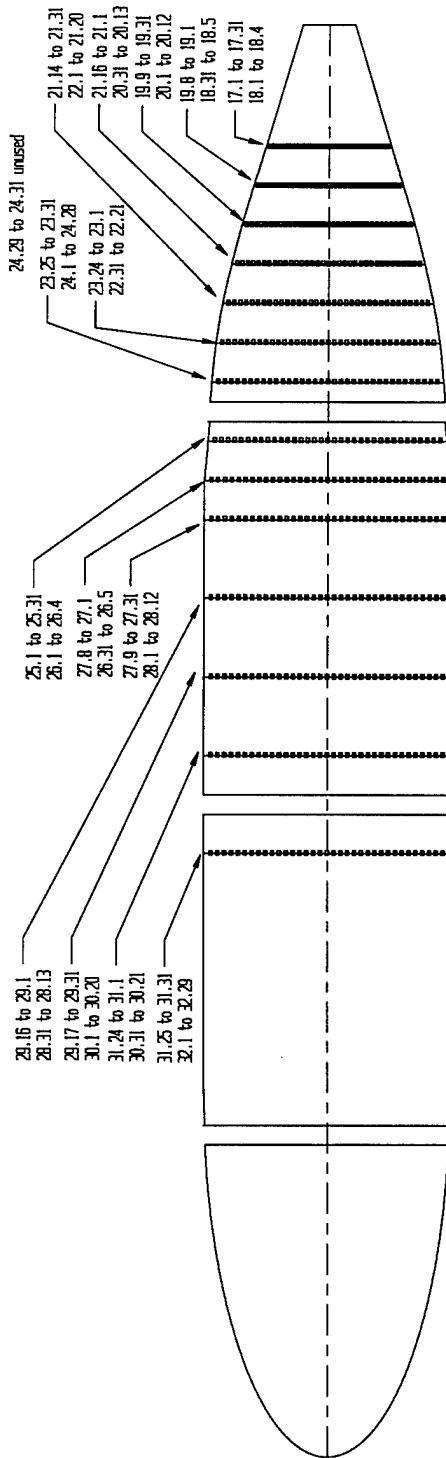
16.25 to 16.1
15.31 to 15.22

16.23 to 16.31 unused

Figure 18. Sensor map.

Sensor application was very labor-intensive and was carried out primarily by two undergraduate students at Virginia Tech. The steps are as follows:

1. Sensor area preparation: The sensor area is sanded with 400 grit paper and cleaned with a degreaser to improve adhesion (Figure 19).

2. Sensor alignment: The sensors are individually installed on the model in the desired position with cellophane tape. Then the tape is pealed back, with the sensor still attached to the tape and the tape base still attached to the model (Figure 20). Therefore, the sensor back and model surface are exposed for adhesive application and the sensor is aligned via the tape. This is a standard strain-gage installation technique.

3. Surface primed: Measurements Group M-Bond 200 Catalyst-B surface primer is applied to both the sensor backing and the model surface and allowed to dry (Figure 21).

4. Adhesive applied: Measurements Group M-Bond-200 room-temperature-cured adhesive is applied in a small stripe where the edge of the sensor meets the model surface. This adhesive is very thin, and thus spreads very easily. Using the tape, the sensor is pulled down tight to the model surface. The tape guarantees the sensor will go to the desired position and orientation, which is critical because the adhesive is cyanoacrylate-based and thus cures almost instantly when the sensor contacts the model surface. As the sensor is pulled into position with the tape, the sensor is pushed down with a thumb in order to squeeze out as much adhesive as possible. The translucent sensor backing makes it possible to judge whether or not the adhesive has adequately spread to all parts of the sensor. Sensors in which the adhesive has not completely covered the sensor backing are replaced (Figure 22).

5. Wire holes drilled: With the tape still on the sensors as a protectant, the holes for the individual wires are drilled in the fiberglass surface (Figure 23). The pattern for determining where holes are drilled is based on whole strings of sensors (all sensors common to a given current source) and *not* on model rings. For a 31-sensor string, a hole (and thus a wire) is drilled in between each sensor, and two holes (for two wires) are drilled on the string ends, for a total of 34 holes (conductors). The extra wires on the string ends deliver the current to the string. The remaining 32 conductors provide differential voltage leads for the 31 sensors. The holes are drilled with a hand drill and a 3/32" drill bit. Most of the holes are located directly between pairs of sensors. In some cases, hardware behind the model skin required moving the wire holes several inches away from the sensors. Also, in cases were a string was distributed between two rings, an extra pair of holes was needed to provide for a wire to connect the two sub-strings in series.

6. Wire holes dremeled: Each hole then had a slot dremeled in the top surface of the skin. This slot allows the soldered wire end to be buried below the model surface. The slots were typically 0.1" wide, 0.1" deep, and 0.25" long and were oriented longitudinal to the model on the downstream side of the holes in most cases.

7. Tape removed: The cellophane tape was now removed from the sensors.

8. Install copper foil: Copper foil was used to connect the sensors in series. The 0.001" thick foil was cut in strips 0.125" wide, and were custom cut to length for the individual installations. A length of the foil strip was first anchored in the slot with Superglue (Figure 24). After the glue had dried, the foil is trimmed to length (Figure 25) and rolled to remove creases before soldering (Figure 26). The underside of the strip was fluxed, as were the sensor solder pads. A small amount of solder was applied to the solder pads, the ends of the copper strip were folded down onto, and soldered to, the copper pads (Figure 27).

9. The sensor wires were installed: The cable assemblies (one per string) were installed one at a time. First, the ends were sorted by color and inserted through the holes until all 34 conductors were in place. The redundancy of the colors is dealt with by the fact the conductors are ordered in twisted pairs, thus there are no two wire pairs that are alike. After all of the individual conductors were inserted in the holes, each wire was cut to length, had 0.25" of insulation stripped from its end, and was tinned. The copper foil in the slot was fluxed and tinned. The tinned wire end was bent over by more than 90° (to form an acute angle between the wire and its tinned end). The wire was then pulled back through the hole until the tinned end touched the foil in the slot. The wire was finally soldered to the foil.

10. First sensor test: All of the sensors were then tested with a multimeter to ensure full continuity. Any faulty sensors or wires were repaired or replaced.

11. Wire holes filled: Each wire hole was filled with Boatlife Life Seal Waterproof Polyurethane/Silicone. This silicone is designed for underwater applications. The silicone was forced from the outside model surface to the inside to guarantee the entire hole was filled.

12. Cables routed in model: The signal cables were then fastened to the model on the inside with 1"x3" sheet metal plates that were attached with 3/16" long sheet metal screws tapped into the fiberglass. This strain-relieved the cables and strategically routed them to be as neat as possible.

13. Sensors checked again: Any faulty sensors were replaced.

14. Sensors and model prepared for waterproofing: The model was sanded around the sensors to improve adhesion, but for fear of risking damaging sensors, sanding was done no closer than 0.25" to the sensors. Then the entire model was washed with acetone twice so the surface would be chemically clean.

15. Application of first "waterproofing" - Masterbond EP21ANLV: Masterbond EP21ANLV adhesive had been selected during the original project as the waterproofing coating due to its high thermal conductivity. It was specified that scotch tape should be placed on either side of each sensor ring to serve as a thickness guide; that the Masterbond should be applied between the pieces of tape; and that a razor blade should then be dragged along the tape to smooth out the Masterbond and guarantee a uniform thickness. This was first tried on a test panel of sensors. It was found that the Masterbond was too thick and grainy, and that when one tried to drag it out into thin layers the grains in the adhesive

(which, incidentally, are what give it a high thermal conductivity) scraped clean in small streaks, leaving the sensors partially exposed. It was found that three layers of tape (total 0.021" thick) were required to guarantee a contiguous, fully sealed surface. The additional thickness thus entailed effectively negated any positive effect due to the high thermal conductivity of the MasterBond material. Regardless, the MasterBond was applied to the sensors. After the entire model was done, the tape was to be pulled off to leave the MasterBond alone. While pulling off the tape, the MasterBond chipped off in huge pieces, indicating very poor adhesion to the model. It was decided that the Masterbond would not make a suitable waterproofer, so the Masterbond was removed by carefully chipping it away from the sensors. Remarkably, and as a testament to the ruggedness of these sensors, none of the nearly one thousand sensors were damaged during this process. However, it was found that at several locations that Masterbond did actually adhere well to the sensors themselves, so approximately 25% of the sensors were left with MasterBond as a coating.

16. Application of second "waterproofer" - FibreGlast Neutral Gel Coat: The authors were faced with the task of completely re-designing the waterproofing and installing it in the last 48 hours before delivering the model. After discussing several options, it was determined that polyester gel coat would be the best option, since the model was most likely constructed with polyester resin (thus adhesion should be good; even if the model was constructed with epoxy-based resins, adhesion should still be good), and since the authors had enough gel coat in stock from other projects. The gel coat was brushed on in three coats. It was noted at several locations that the second coat of gel coat "bubbled up", indicating locally poor adhesion between the different layers of gelcoat.

17. Final sensor check: The sensors were all checked one last time, and all were fully operational.

The model was then delivered to the model fabricators where final fitting of some external components. The following photographs illustrate some of the steps.
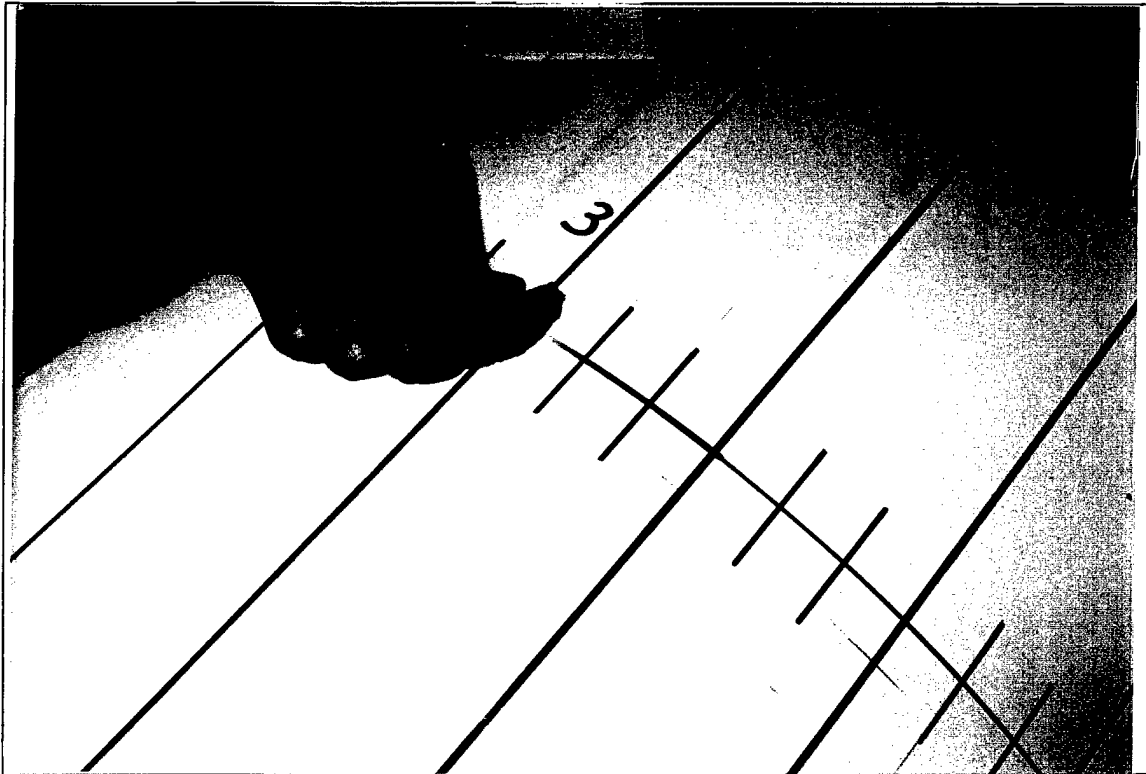
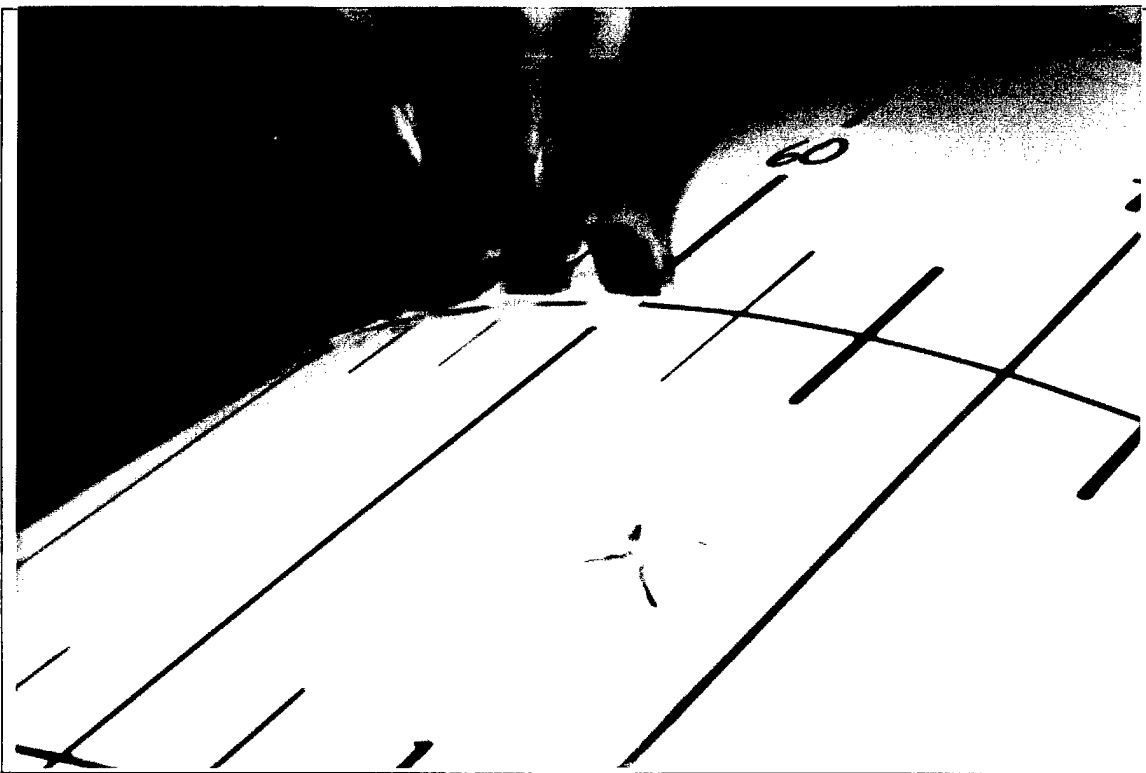Figure 19. Sanding all locations where sensors are to be bonded.

Figure 20. Sensors aligned with scotch tape.

Figure 21. Application of primer to sensors and model. After the primer is dry, adhesive is applied and the sensor is "hinged" down into place using the scotch tape and anchor.
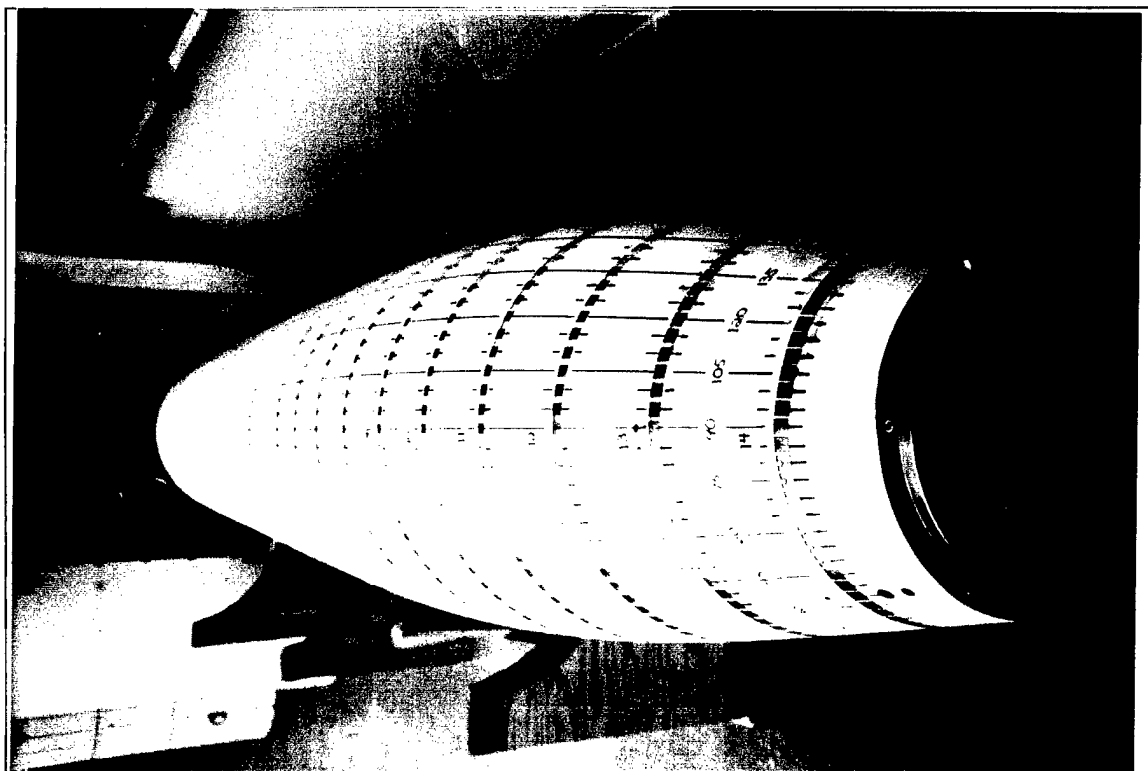

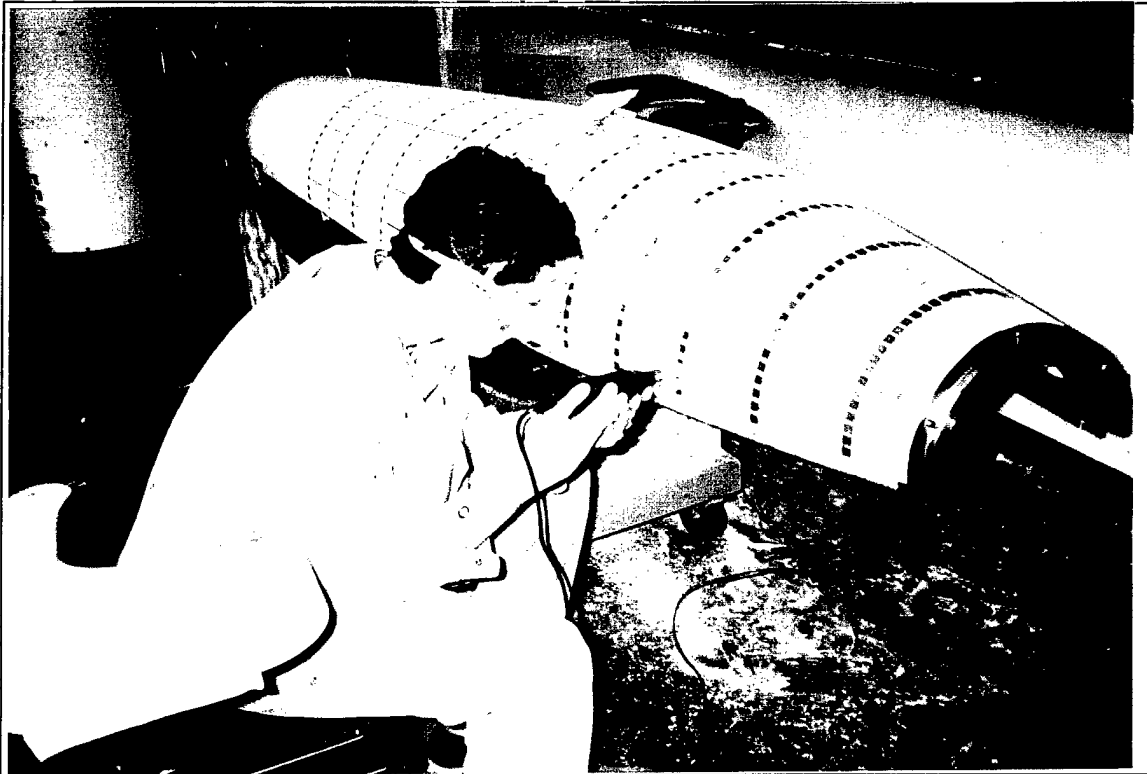Figure 22. All of the sensors glues on the bottom half of the model.

Figure 23. After all the sensors are glued in place, holes are drilled for the lead wires and slots are "Dremeled" into the model surface where the leads will be buried.

Figure 24. The copper foil strips are "superglued" into the slots to temporarily hold them in place while the foil is soldered to the sensors.
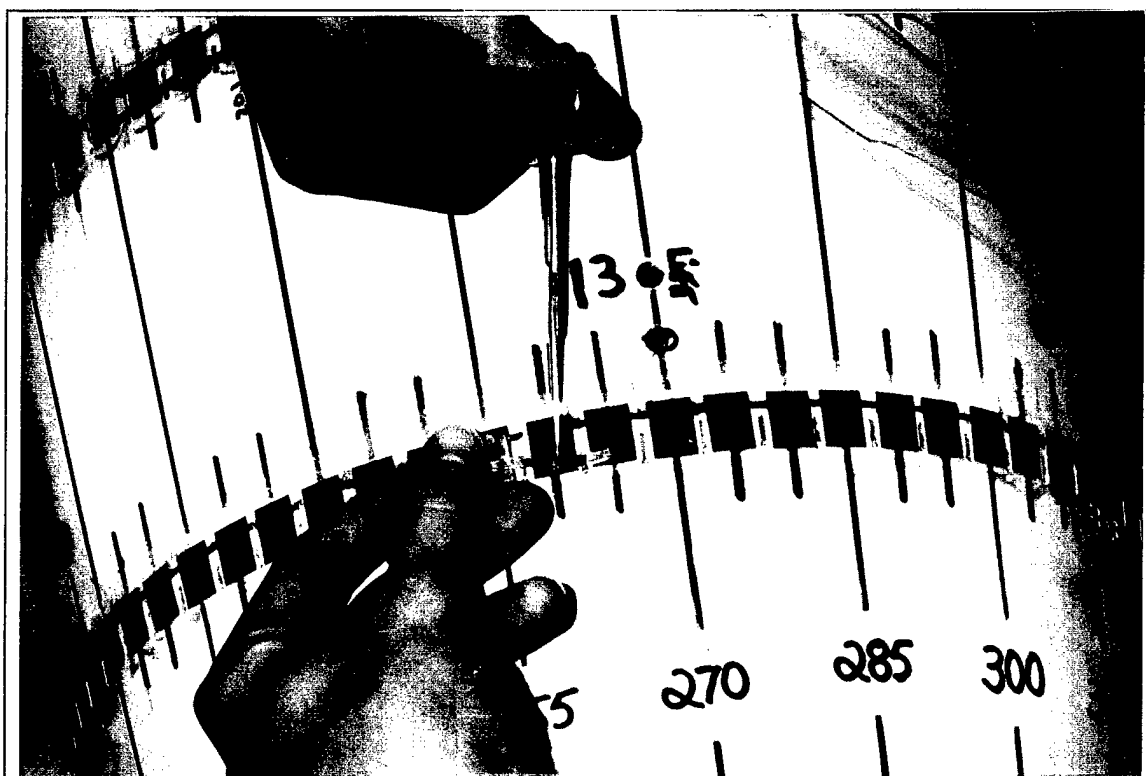
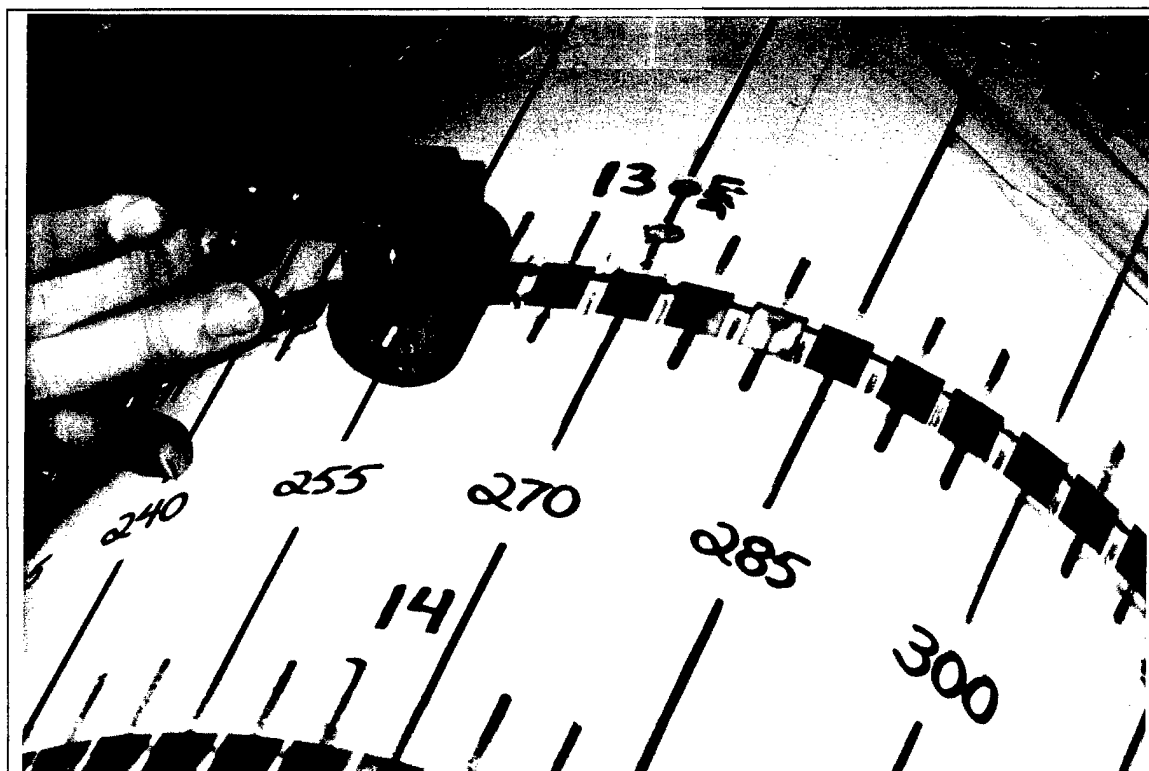Figure 25. The foil is trimmed to length.

Figure 26. The foil is rolled flat to take out any creases before soldering.
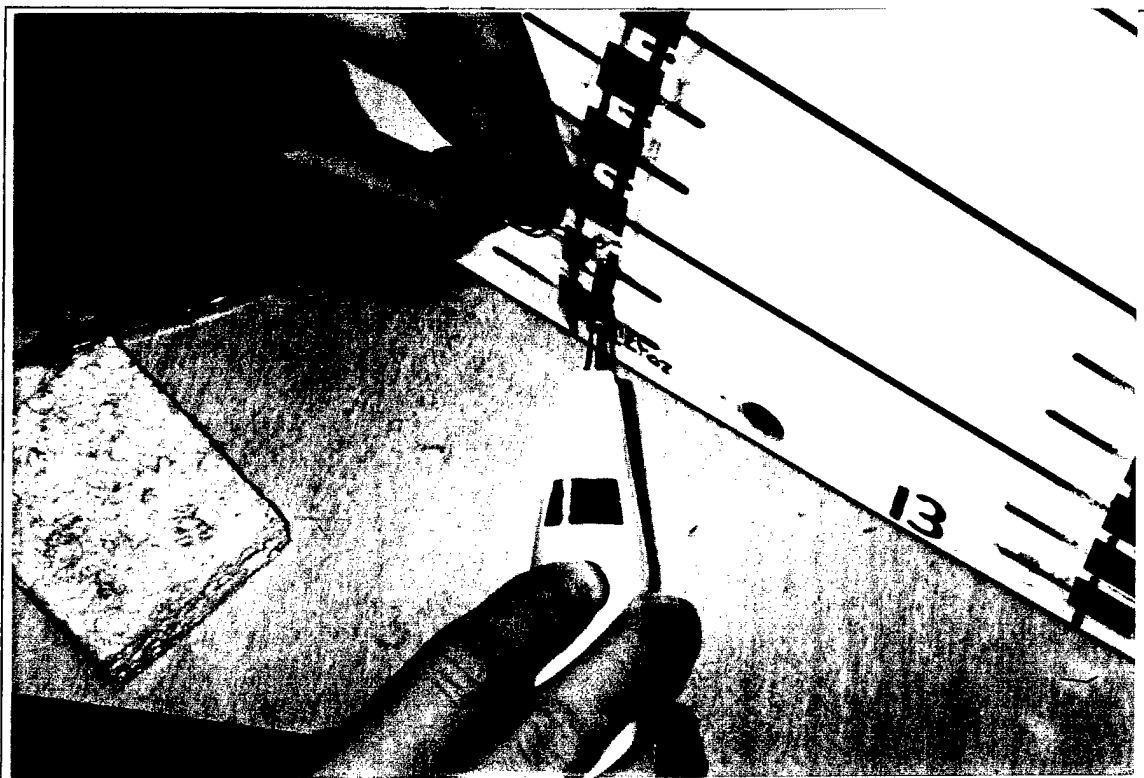
Figure 27. After fluxing both the copper and the sensor, the foil is soldered to the sensor.

Model Basin Entry #1: April 10-26 1995

Upon arrival at the Model Basin for the first entry, the sensors were first checked for faulty sensors. Several broken wires were found and repaired. No sensors needed to be replaced. The sensors were also inspected for regions where the waterproofing was deemed weak, and touched up locally several times to improve the probability that the waterproofing would work. The electronics were unpacked and hooked up to the computer. All of the boards were operating nominally. A broken connector that plugs into the computer was repaired.

Next, the box was installed in the model and the boards were inserted in the box. The boards were hooked up to the sensors on the model. The boards were hooked up one board at a time because when testing them out, it is important to monitor the electronics to make sure that no sensors are being burned out by faulty electronics. In order to minimize the number of sensors one has to be watching at a time, the boards are powered up one at a time.

The first board checked out divulged a new quirk in the boards. Originally, all of the boards were hooked up to the sensors and to the MUX board, but the power cables were disconnected on all of the boards except the one being tested. It was found that having unpowered boards hooked up to the digital electronics that selected MUX addresses makes the digital electronics, and thus the one powered board, fail. Therefore, it was found that it is important to have any unpowered boards completely disconnected from the system during operation.

This first checkout determined that all boards and sensors were working properly. However, board number 7 did have an intermittent problem whereby sometimes the voltages being measured on the sensors was lower than expected. Efforts to pin down the problem failed since it was not repeatable.

After fully assembling the system, it was determined that the box, which straddled the sting, would hit the sting under extreme model deflections. Considering the box was made of Plexiglas, it was determined that the setup was entirely unacceptable. It was also determined, however, that there was more than enough room in the nose to house the electronics, and that the sensor cables were plenty long enough to reach to the nose. A shelf was constructed and fitted in the nose. The box and boards were completely disassembled and reassembled in the new nose mounting region. The box and its installation are shown in Figure 28 below.
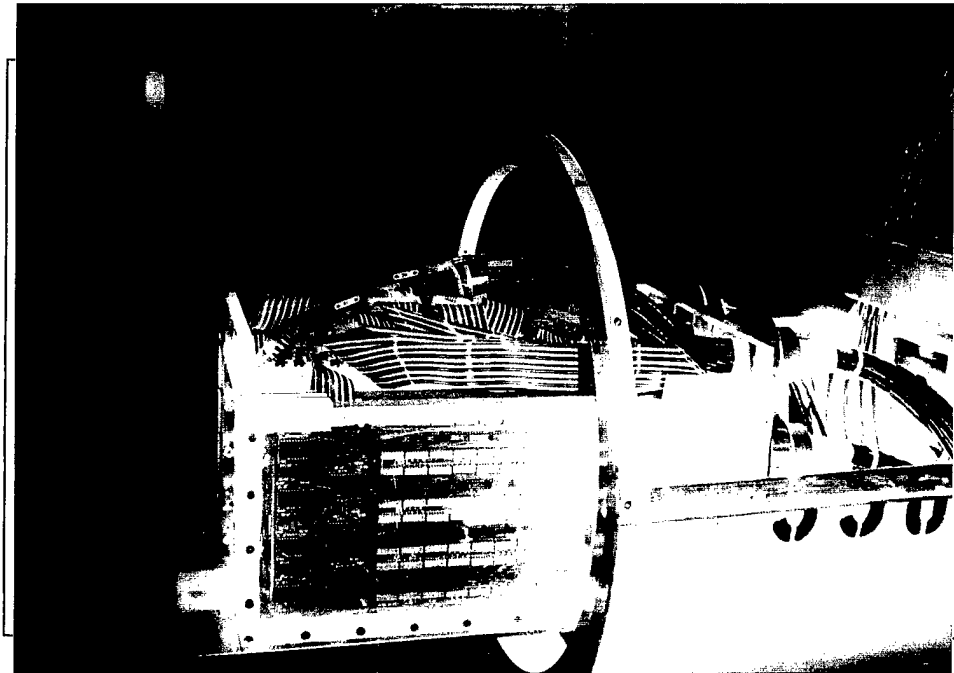

Figure 28a. The boards and all cables connected in the anemometer housing, now installed in the model nose.
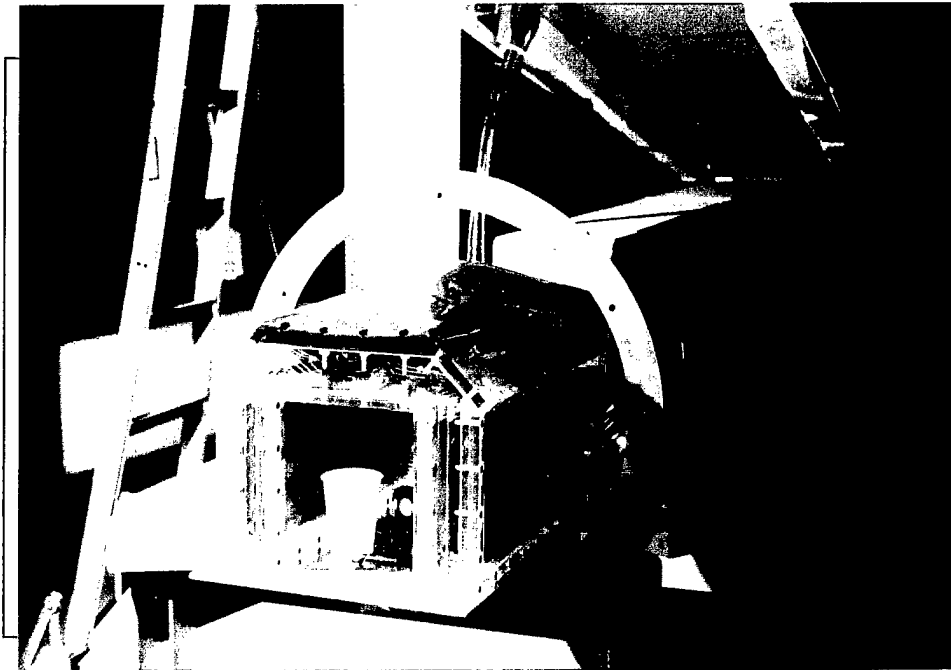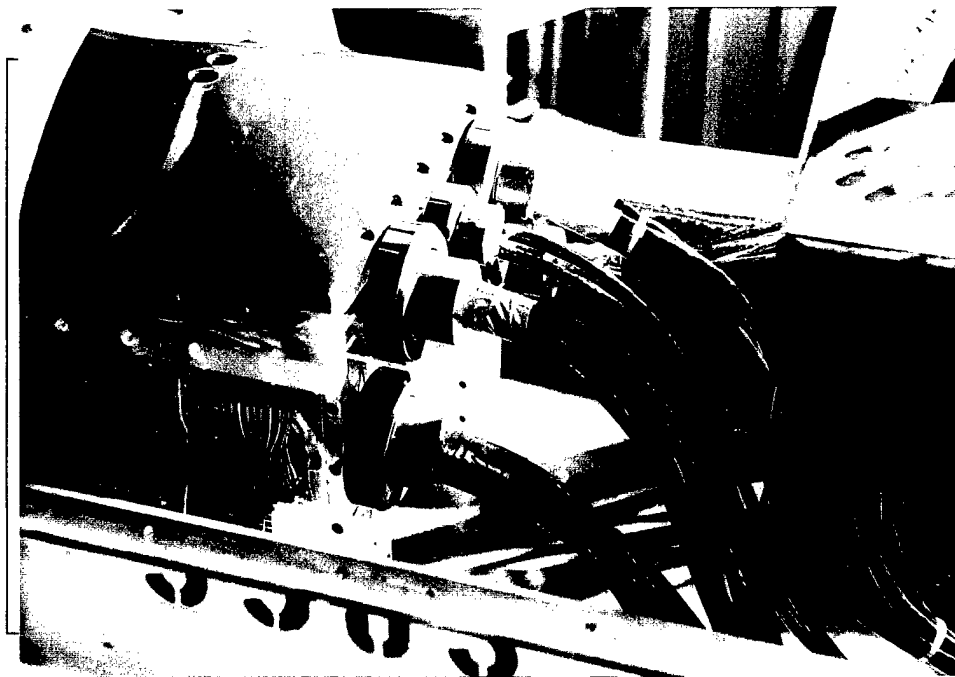
Figure 28b. The lid installed on the box.

Figure 28c. The orientation of all of the cables exiting the box.

At this point the SylGuard gel that was to be used inside the box was abandoned, because it was felt that there would be a need to remove the boards several more times, and the gel would provide a terrible mess to be cleaned when needing access to the boards.

After rechecking the entire system again and finding no sensor problems, the box lid was glued into place with the waterproof silicone and bolted down. After the lid was glued down, two sensors failed. It was found,

however, that the problem was in solder joints on the model surface. These were repaired and resealed. The model was lowered into dry-dock. Figure 29 shows the fully rigged model prepared for dry-dock.
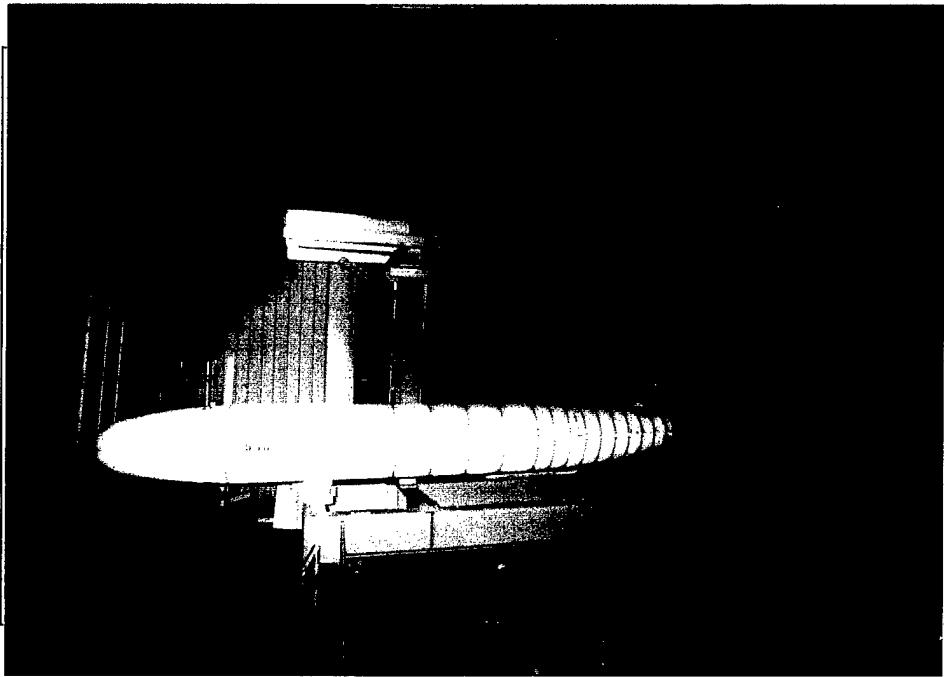

Figure 29. The model, fully rigged, prepared to be lowered into dry-dock.

The next day several other electronic failures occurred. The box was reopened, and the various problems were debugged and repaired. The box was resealed. After resealing the box, it was check for leaks by either pressurizing the air inside the box or applying a vacuum to the inside of the box through a hole in the box lid. Several leaks were found on the box. The largest leak was suspected to be coming from the PVC connectors that housed the signal cables potted in Silicone. The box bas disassembled again, the cables were removed again, most of the silicone was removed, and the cables were repotted with ACME Maraglass Casting Epoxy by DTRC personnel. After reassembling the box, additional leaks were found in the box itself, and these were sealed with additional silicone or casting epoxy.

At this point, the model was partially lowered into the water with the sensors powered up. Three sensors burned out. It was suspected that this was because the sensors were powered while they were being submerged, and that this might have shocked the system somehow. So the power was turned off, and the model was completely submerged. The power was turned on and the current sources set to roughly 100 mA. The system was run for roughly 45 minutes, during which time sensors burned out on roughly 75% of the strings. In most cases, it was only one or two sensors burned out on a given string. The power was shut off, the model was raised out of the water, and the sensors were inspected.

Several failure modes were observed (see Figure 30). In general, the gel coat did not adequately waterproof the sensors. The worst failure was that the edges of at least 75% of the copper foil was corroded green, indicating the gel coat was too thin to adhere to the sharp (0.001" thick) foil edges. This provided a conductivity path for the sensor

current to escape to the water, allowing too much current to flow through selected sensors and burn them out. Any burned out sensors were burned out on very tiny individual portions of the sensors. This is different from burning out in air, where typically the entire sensing area gets completely burned out.

A few sensors actually had some corrosion directly on them too, typically white or brown colored. These were probably locations where the gel coat did not adequately cover the sensors.

In general, locations where sensors were still covered with MasterBond had the fewest failures, although there were several areas where the MasterBond broke down in the presence of water, converting into a brown, thick pasty substance, and losing all solidity.

At this point, the waterproofing problems were deemed too serious to repair on site. The electronics were removed, the cable ends were sealed in PVC tubes, and the force and moment tests were performed as planned.
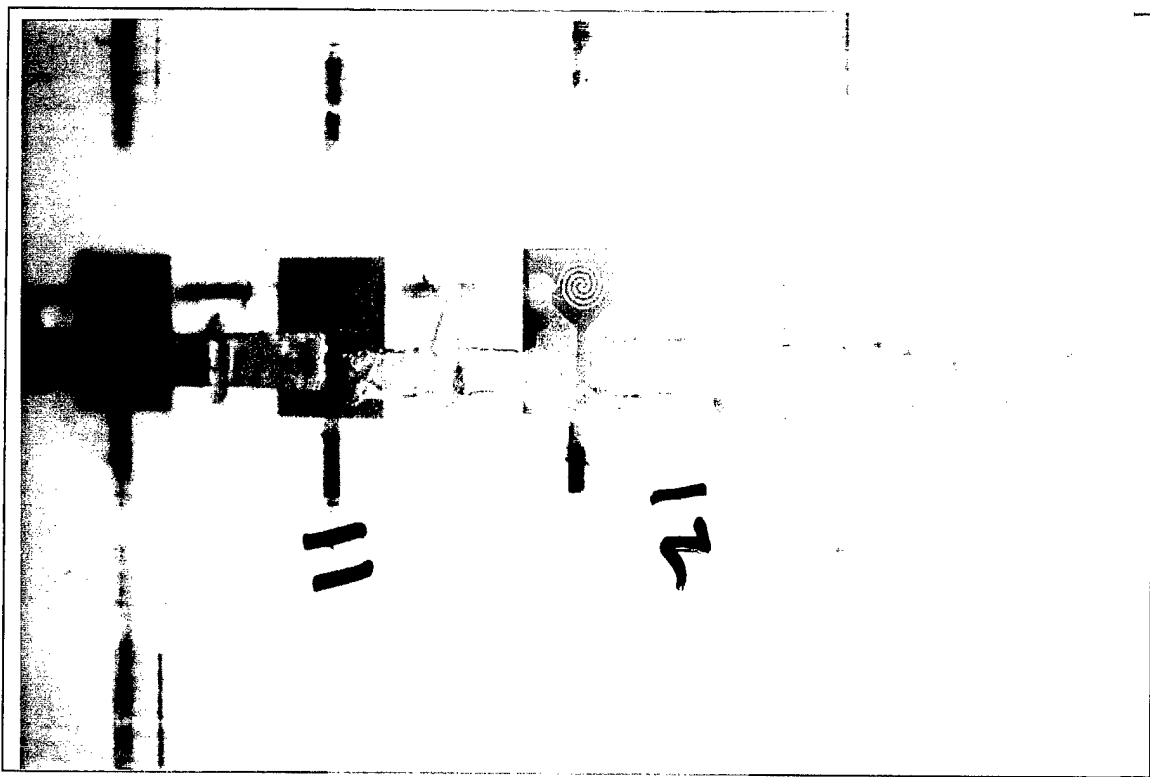
Figure 30a. Waterproofing failure modes. This was the most common: corrosion of the copper foil, resulting in a greenish-blue oxide on the edges of the copper foil, where apparently the gelcoat did not completely cover.

Figure 30b. Waterproofing failure modes. In some places where the copper was soldered to the sensor, this white corrosion, assumed to be a lead oxide, was found.

Figure 30c. Waterproofing failure modes. Several sensors exhibited these brown spots, which are regions where the foil material apparently either burned away or the brown is an oxide of the iron in the BALCO foil.

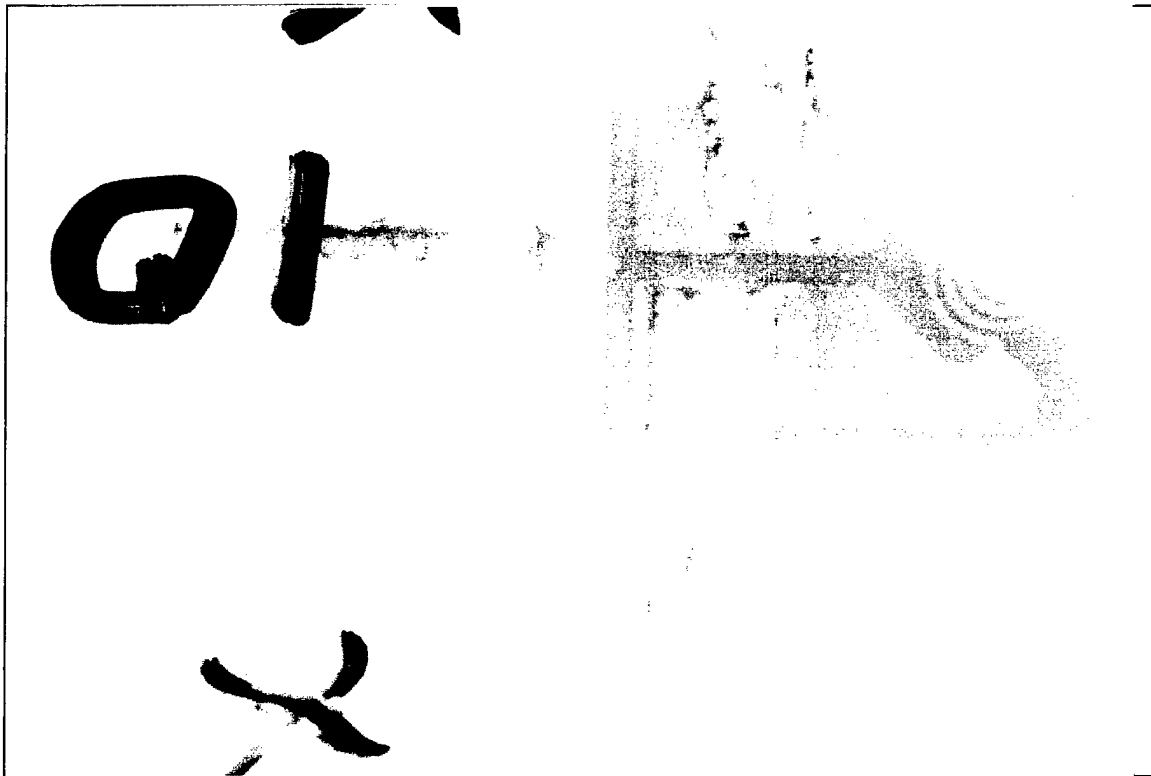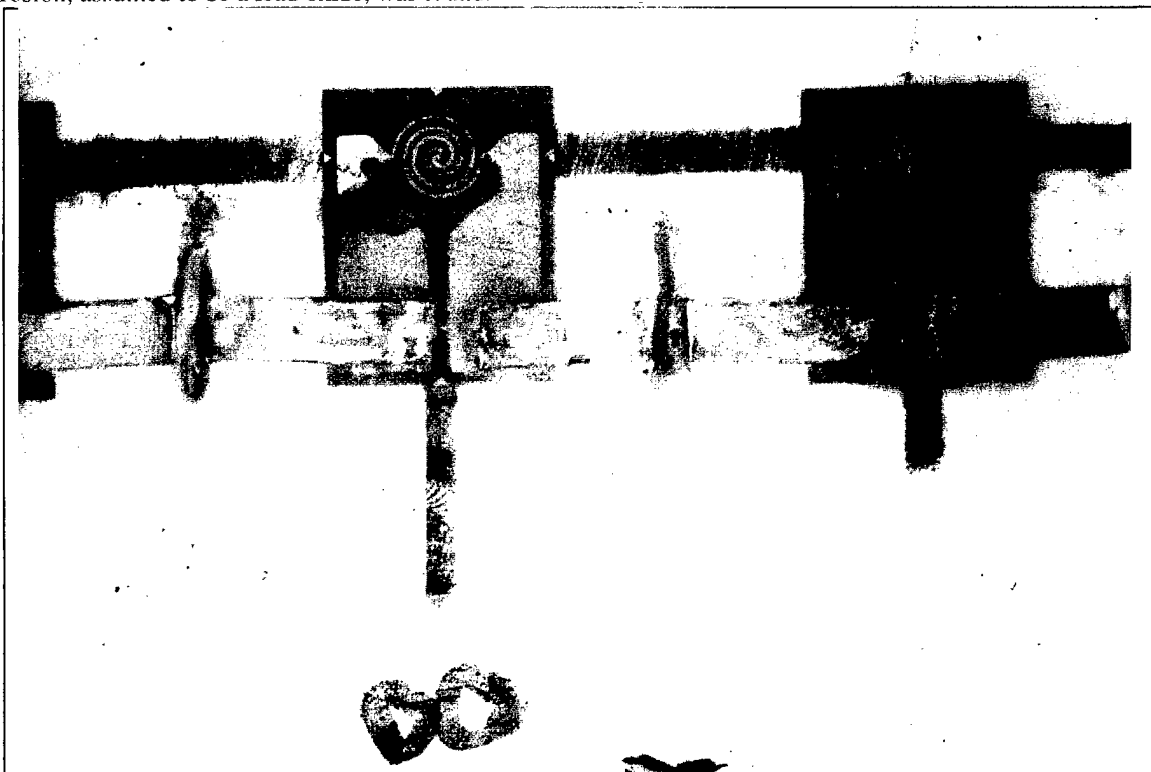Figure 30d. Waterproofing failure modes. Another all too common failure mode was the wrinkling up of the gelcoat waterproofing material, indicating contamination on the model surface due to incomplete surface preparation.

System Changes

Many modifications were made during the time between the two Model Basin entries. First, a new box was designed and built. It was made into a simple rectangular box shape since it no longer had to straddle the sting (Figure 31). It was constructed out of 0.5" thick aluminum, with all seams sealed with Permatex Form-A-Gasket No. 1 except the lid, which was sealed with a gasket. The box was tested numerous times underwater, with the lid being removed and replaced repeatedly, until enough confidence had been built up as to permit box assembly without testing for leaks. The boards were spaced out slightly more inside the new box.

When unsealing the connector ends of the signals cables, it was found that the PVC vessels that housed these connectors were filled with water. Since it was deemed unlikely that the PVC joints had leaked, it was assumed that the water had wicked up the signal cables in between the individual conductors via capillary action. This should not have happened because specifications for the cables constructed by Mercury wire called for adequate blocking at the exposed end to prevent taking on water. A spare cable was dissected to inspect the quality of the waterproofing done by the cable manufacturer, and it was found that the construction quality was unacceptably low. Therefore, molds were constructed to pot the cable ends with Acme MaraGlass in the exact same fashion as done by the DTRC personnel on the box connectors earlier. All 32 cables were resealed in this fashion.

While repairing the sensors on the model, a test panel of sensors was installed on a PVC pipe, coated with the MasterBond and gel coat, and run until failure in a small water tunnel at Virginia Tech. Then, two different types of rubberized coatings were applied to the model. The first was PRC-1005 rubber coating as suggested by DTRC

50

personnel. This worked very well, but it was deemed necessary that any coating should be sprayed on to minimize coating thickness. Spraying equipment would have been expensive for this particular rubber. Also, there was a prohibitively long lead time on acquiring enough of this particular coating. Alternatively, a commercially available rubber coating, Spray Tool Dip, was found that had similar sealing properties but came in a spray can and was readily available. This was applied to the sensors, and proved adequate for waterproofing. Details of this study were described in a memo released in June, 1995, entitled *Interim Report: Waterproofing Hotfilm Sensors for Underwater Use*, which is included in Appendix A. Among the findings were that the sensors did seem to indicate separation properly, although the results were no where near as good as had been seen in the wind tunnel experiments.
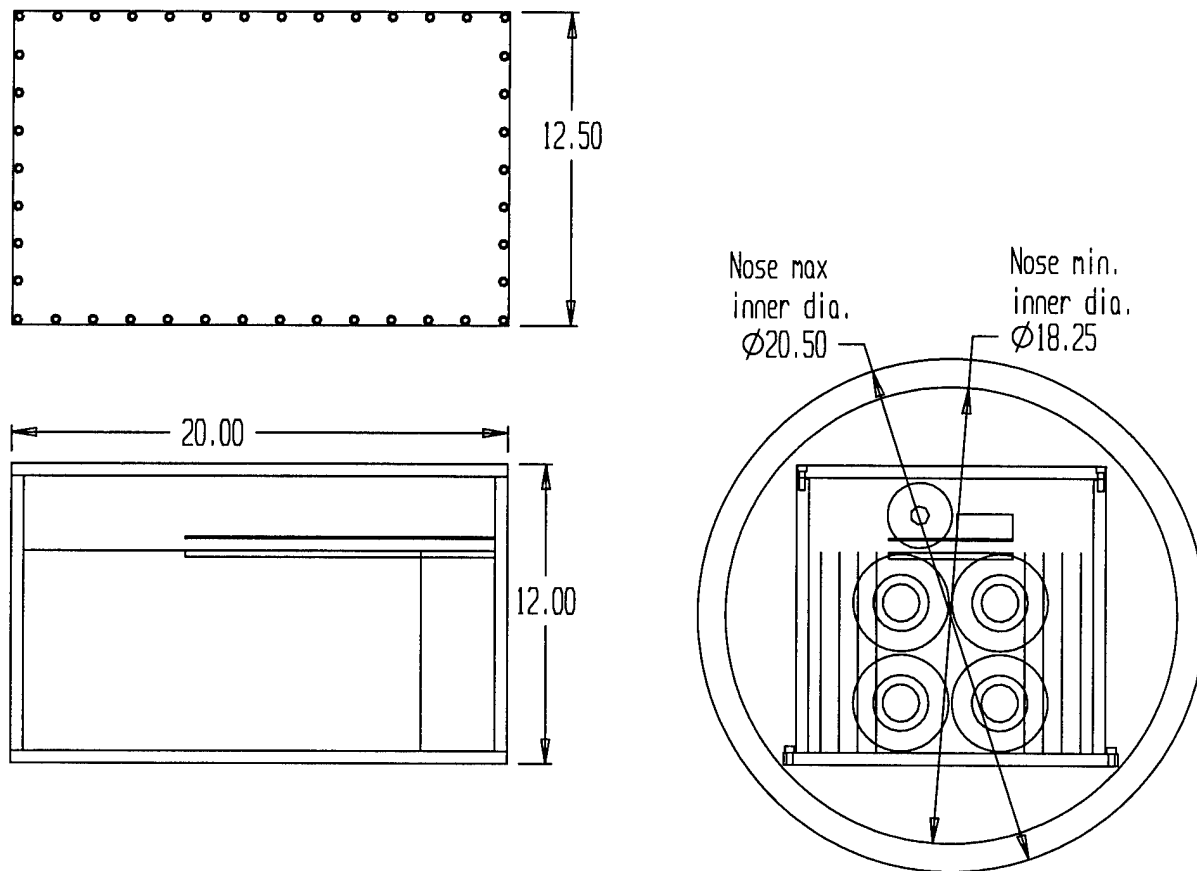
Figure 31. New anemometer housing.

All of the gel coat was meticulously removed from the model and sensors, and all remaining MasterBond was removed as well. This was done using razor blade scrapers, X-Acto knives, etc. This was a very labor intensive step, and as much of the old material was removed as possible. All burned out sensors were replaced, and the sensors were all inspected several times for weak sensors. Any sensor with any damage whatsoever to the sensing area was replaced. Similarly, all weak copper foil pieces were replaced. A Dremel Moto-Flex Tool (Model 332) was used to sand the fiberglass surrounding all of the sensor strings to improve adhesion between the waterproof coating and the model surface. This tool allowed the user to sand right up to the edge of the sensor without fearing damaging the

sensors. After removal of the gel-coat and Master Bond epoxy, the model was opened up and cleaned with a pressure washer. This removed the rust that had developed from the steel cable tie-down straps and other dirt that had collected inside the model. The steel tie-down straps were replaced with plastic anchors (fastened with stainless screws) and small tie wraps. The areas adjacent to the interior wire leads were sanded in preparation for spraying at a later date. A Ryobi detail sander was used for this purpose.

The tail was coated with the waterproofing first to test the entire application technique. The sensors and foil were then etched with Naval Jelly, and were cleaned with Acryli-Clean degreaser to prepare for spray rubber application. The interior and exterior of the model were then masked in preparation for spraying. The spray tool dip was sprayed on the model in moderately heavy coats. This method of application caused the coating to pit, and the rubber would not cover small existing holes on the model's surface. Heavier applications of the spray rubber only made the problem worse. The initial rubber coating was removed and an epoxy filler was used to fill the holes. Repeated light applications of the spray rubber worked well. If applied too heavily, the spray rubber would act as a solvent and loosen large areas of rubber. About 12 light coats of rubber were used on the exterior of the tail lid. Around coat number 8, the brush-on tool dip was used to repair problem areas and pinholes. The interior of the model was sprayed with about 6 slightly heavier coats. This inner application was considered only a secondary water barrier, since the interior wire leads were already potted using silicon rubber.

Since the spray rubber formed a strong sheet that would peel away, the exterior masking was removed using a razor blade. A plywood tank was constructed, lined with a swimming pool liner, and filled with water. With the masking removed, the tail lid section was put under water and tested. After a period of several days, the system performed satisfactorily, and we proceeded with the remaining parts of the model. (Note: During this testing, a stream of water was held on different individual sensors to determine if the raw voltage signals would indicate the sensor with the additional cooling. This test was not successful.)

Waterproofing of the rest of the model continued based on the success of the tail lid section. The main lid was stood on end to paint, and the main body was painted while on its carriage. Approximately 10 coats of spray rubber went on the model exterior, 5 coats on the interior. Areas with poor coverage were hand-brushed twice during the spraying, and almost the entire copper foil area was brushed at least once. The waterproofing/painting process took about 10 days.

The entire model was submerged in the water, and the sensors were powered up at 100 mA. The objective was to run the sensors for one hour straight with no failures. After about 50 minutes, several sensors burned out on one string. Several iterations of repairing sensors, submerging the model, and running the anemometers were completed before it was realized that the boards themselves were being overstressed. Several repairs were made to the boards to make them more robust, but it was also determined that the 1 hour test was too stringent, since normal operation at the Model Basin would only require runs of a total of 1 or 2 minutes maximum length with no current on, 15 seconds with the current actually on, and 15 minutes of cooling in between. Using a test with similar amounts of on and off time, the system performed properly for over 24 hours under water, at which point the system was deemed ready for use. It was then delivered to the Model Basin.

Model Basin Entry #2: October 18-26, 1995

The model and electronics were delivered to the model basin on the evening of the 18th of October. Thursday morning, the model was unloaded, and the Model Basin crew began to rig the model on the sting. On Friday, the model was ready to be put into dry dock in preparation for attaching it to the rotating arm. All electronics were connected including a water intrusion alarm ("sonalarm") supplied by John Bedel and installed in the electronics housing. After connecting, the sonalarm in the electronics box went off. This turned out to be a false alarm, caused by the conductivity of gasket material in the bottom of the box. The sonalarm detection wires were properly insulated from the box floor and re-tested before re-sealing the box lid. The model was attached to the rotating arm successfully, but one of the gauge block was broken. It was late in the afternoon at this point, so we returned to Blacksburg for the weekend.

John Bedel had figured out a way to replace the bad gauge block with minimal effort, so on Monday morning he completed that task. We spent our time fixing some electrical problems, and by the afternoon everyone was ready to perform some test calibration runs. The model was moved in to a minimum radius configuration, with a yaw angle of approximately 13 degrees (nose out). About 4 test runs were made late that afternoon to check the repeatability of the data and the differences between individual sensors.

On Tuesday morning, some more test runs were performed, but with discouraging results. Repeatability could be achieved if sensors were warmed up properly (reached a steady state condition), but the data in general did not show distinct separation locations, and looked quite noisy in general. These test runs were tried:

- tight radius, yaw angle of 13°, $U_\infty = 5$ knots

- large radius, yaw angle of 25° (maybe larger), $U_\infty = 5$ knots

- large radius, yaw angle of 0°, $U_\infty = 5$ knots, 0.5 knots, 0.005 knots

A quick analysis of the sensor cooling problem revealed the main problem: the sensitivity of the sensors in water was about 250 times smaller than in air for the same current settings. After extensive consultations, a decision was made to try and modify the electronics in an attempt to show that a hot-film system could detect separation. The plan was to reduce the number of sensors in a given string and to increase the current going through the sensors. The op amp resistor chips would also have to be changed.

The way to know whether the anemometer system is capable of properly heating up a sensor is to use as much current as possible and try to purposefully burn out a sensor. An attempt to burn out a test sensor in water was the first job for Thursday morning. We could not burn out the sensor, but did manage to burn out some current sources. The current sources simply were not stable at the higher settings (about 0.6-0.7 amps). We actually needed more than 1 amp for any hope of success and the existing current source design was not capable of such amperage, so plans to modify the electronics were scrapped. The model was derigged and the electronics removed. Thursday afternoon we returned to Blacksburg.

Suggestions for Future Improvements

Current Leakage

Presently, the relatively low impedance of the amplifier circuits allows a small but significant current, or "leakage current", to flow out of the sensor string and through the amplifier circuits. The successive leakage of current through each of the 32 amplifier circuits in a string results in significant deviations of the actual sensor current from that set by the current source; moreover, this implies that each sensor is at a slightly different current. As a result, each sensor current must be estimated using simple circuit analysis; but this crucial step in the data reduction means that the *current and thus the resistance for each sensor is dependent on the voltage of each of the other sensors in the same string*. Aside from drastically complicating data reduction and significantly increasing measurement uncertainties, this also means that if a failure occurs on one sensor in a string (or that sensor's circuitry), accurate data reduction becomes impossible.

Future designs should attempt to eliminate significant leakage currents. This requires increasing the amplifier circuit impedance by at least a factor of ten. This is most easily accomplished by increasing the resistances in the amplifier circuits by a factor of ten (keeping their ratio constant). However, using such high resistances can sometimes lead to stray amplifier offset voltages due to the small but finite current ("bias current") which runs into the amplifier inputs. To counter this problem, op-amps must be selected that are specifically designed to have an ultra low input bias current.

Stability of current sources

The constant current sources are not constant or repeatable enough in the current design. Therefore, one channel of every 32-sensor string was dedicated to a very high precision resistor sampling the string current directly. This results in only 31 live sensors per string, along with one fixed resistor. If possible, current sources repeatable and stable to within at least 0.1 mA are required. Otherwise, the current sources will always have to be sampled, thus tying up channels on the system.

Accuracy of amplifier circuits

The amplifier circuits on these boards required being individually calibrated for exact gains and offsets. This is very labor intensive on a system with 1024 amplifiers. In the future, resistors with at least 0.1% repeatability (preferably 0.01% repeatability) should be used to obtain uniform gains. Also, very high quality op-amps should be selected to minimize offsets. Despite the fact that these components largely drive the cost of the boards, extra money spent will significantly decrease the labor and complexity of using the boards, interchanging boards, and reducing the data.

MUX cross talk

In the current board design, typical circuit failures result in very high or low incorrect voltages presented to the multiplexers. In the current design, these extreme voltages corrupt the multiplexer output voltages on otherwise properly working channels. Therefore, typically one bad voltage actually made 2 entire boards non-operational. The multiplexer circuits need to be protected from erroneous voltages.

Modular electronics

The anemometer boards were not designed to be easily connected or disconnected or switched. In all future designs, the anemometer board should be designed to incorporate the smallest common denominator of parts and be totally capable of being easily replaced by an identical board. Such a level of modularity will make development, testing, and repair much easier. In addition, the boards should be designed to be completely interchangeable without requiring any re-calibration.

Number of sensors in a model ring equal number of sensors in a board string.

Mapping of the sensors from "board coordinates" to "model coordinates" is much easier if the number of sensors in a model ring is an equal multiple of the number of sensors on a given board. Wiring is also facilitated if strings on a given board do not have to span two model rings.

Mechanical Design

A disproportionate number of failures, and lots of engineering headaches, were due to deficient board mechanical design. To save cost on board construction and design, a two-sided circuit board construction was selected. This resulted in a tremendous number of very fragile wires completing many of the circuits. Also, all signal cables were soldered directly to the boards, with no provisions made for strain relief. In the future, the boards should be designed with no cables or wires soldered directly to the boards at all. This will require at least a 3 layer, if not a 4-layer, board design. Instead, connectors should be directly mounted to the boards to carry power and signals to and from the boards and to connect the sensors to the boards. A card-edge connector with a motherboard type of configuration should be considered, if possible, to eliminate complex cable routing.

On-board A/D converters.

One difficulty in performing these types of measurements in the Model Basin facilities is the fact that the sensors and support electronics are typically a far distance from the data acquisition computer. A large number of *analog* voltages are transmitted over a very long cable length before being digitized by a board in the host computer. In addition, these signals are passed through two multiplexers and various other components before reaching the computer. A more robust design would incorporate A/D converters directly on the anemometer boards. Then, the digital signals could be multiplexed and sent to the host computer, effectively eliminating signal degradation due to extra components and long signal lines. Finally, the effective data rate could be increased significantly due to the fact

that digital, rather than analog, signals are being transmitted. The analog data acquisition board in the host computer should instead be fitted with a much less expensive digital input board.

Similarly, if adequately stable and repeatable current sources are developed, the current source control signal should also be sent digitally to board-mounted D/A converters.

Waterproofing

Despite the fact that the spray tool dip did successfully waterproof the sensors, this was deemed only a temporary fix and not a recommended procedure for the future. Alternative coatings, such as the PRC-1005 rubber coating as suggested by DTRC personnel, should be investigated. In addition, waterproofing options should be considered in the construction of the sensor itself, including possibly a Kapton layer glued over the sensor or a conformal polymeric coating applied after sensor construction.

Sensor Connectors

Although the present connector concept worked, the system will be easier to install if an ultra-high-density connector can be found that allows the cables to be easily connected and disconnected from the box face.

Sensor Design Revisited: Future Potential Hot-film Technologies

The following analyses are included to provide direction for future work in the vein of this report. The existing hot-film sensors do work in air, but the current system does not work in water. The basic physics of heat transfer are exploitable to measure changes in skin friction, but any design of this type of measurement system must account for all aspects of the entire system, from modeling the behavior of the sensors in the water to determining the real uncertainties of the final reduced quantities. The body of work presented in this report provides a wealth of experiences upon which to guide such a next-generation design.

Sensor Heat Transfer to Fluid

The analysis provided in Simpson et. al. (1991) that shows the relationship between film coefficient and velocity gradient is still valid. It is repeated here for reference:

$$h = \frac{3}{2} \frac{Mk\left(\partial U/\partial y\right)_w^{\frac{1}{3}}}{\left(3\alpha l\right)^{\frac{1}{3}}}$$

where M is a constant (1.12), k is the thermal conductivity of the fluid, α is the thermal diffusivity ($k/\rho c_p$), and l is a representative sensor length in the local near-wall flow direction. Substituting in for the velocity gradient in terms of a skin friction coefficient and the basic fluid properties in place of the thermal diffusivity yields:

$$h = 1.165\left[\frac{C_f k^2 \rho^2 U_\infty^2 c_p}{2l\mu}\right]^{\frac{1}{3}}$$

where C_f is the skin friction coefficient, c_p is the specific heat of the fluid, and μ is the fluid viscosity. Assuming a range of skin friction coefficients from 0.001 to 0.010 for these types of flows (Wetzel, 1996), in air the film coefficient will range from 60 to 125 J/(s m^2 °K), while in water the film coefficient will range from 13,000 to 30,000 J/(s m^2 °K). *The difference is two orders of magnitude.*

Constant Current Anemometry

In the existing constant current setup, the sensor current is specified and its voltage is measured as a function of heat transfer and ultimately skin friction. The heat transfer rate is given by

$$\dot{q} = I_s^2 R_s = hA_s\Theta$$

or since $R_s = R_\infty\left(1+\alpha\theta\right)$, then

$$I_s^2 R_\infty\left(1+\alpha\Theta\right) = hA_s\Theta$$

It follows that:

$$\Theta = \frac{I_s^2 R_\infty}{hA_s - \alpha I_s^2 R_\infty}$$

The sensor voltage is determined from:

$$V_s = I_s R_s$$
$$= I_s R_\infty (1 + \alpha \Theta)$$
$$= \frac{h A_s I_s R_\infty}{h A_s - \alpha I_s^2 R_\infty}$$

where I_s is the sensor current, R_s is the sensor resistance, V_s is the sensor voltage, A_s is the effective sensor area, Θ is the temperature difference between the sensor and the free stream, and α in this case is the sensor temperature coefficient of resistivity. It is important to note in this equation that V_s is a *weak* function of h and thus C_f. If one reverses this equation to solve for h in terms of V_s, one gets:

$$h = \frac{\alpha V_s I_s^2 R_\infty}{A_s (V_s - I_s R_\infty)}$$

Again, h is a weak function of V_s. It can be shown in this case that assuming V_s, I_s, and R_∞ are the basic measured quantities, the uncertainty on h can be given as:

$$\frac{\delta h}{h} = \sqrt{\left(\frac{1}{V_s} - \frac{1}{V_\Theta}\right)^2 \delta V_s^2 + \left(\frac{2}{I_s} + \frac{R_\infty}{V_\Theta}\right)^2 \delta I_s^2 + \left(\frac{1}{R_\infty} + \frac{I_s}{V_\Theta}\right)^2 \delta R_\infty^2}$$
$$V_\Theta = \alpha I_s R_\infty \Theta$$

where V_Θ represents essentially the incremental voltage due to the change in temperature of the sensor. Therefore, for the uncertainty on the film coefficient, and thus the skin friction, to be low, the sensor temperature must be high. This requirement is an outgrowth of the denominator in the expression for h above, which makes clear that V_s-$I_s R_\infty$ must not be allowed to approach zero.

The above reduction and uncertainty equations assume that data can be obtained if the sensors are run at only one current instead of several as assumed earlier in this report. The uncertainty relations for computing the film coefficient based on several voltages and currents is repeated:

$$\frac{\delta h}{h} = \frac{1}{r\sqrt{n-1}} \sqrt{\left(\frac{\delta \Theta_{MAX}}{\sigma_\Theta}\right)^2 + \left(\frac{\delta q_{MAX}}{\sigma_q}\right)^2}$$

The uncertainty on q is easily made low, but the uncertainty on Θ is much more difficult to minimize. That uncertainty is repeated thus:

$$\frac{\delta \Theta}{\Theta} = \sqrt{\left(\frac{\delta \alpha}{\alpha}\right)^2 + \frac{\left(\frac{\delta V_s}{V_s}\right)^2 + \left(\frac{\delta I}{I}\right)^2 + \left(\frac{\delta R_\infty}{R_\infty}\right)^2}{\left(1 - \frac{R_\infty}{R_s}\right)^2}}$$

Ignoring uncertainties due to the coefficient of resistivity, after manipulation this uncertainty is

$$\frac{\delta\Theta}{\Theta} = \frac{1+\alpha\Theta}{\alpha\Theta}\sqrt{\left(\frac{\delta V_s}{V_s}\right)^2 + \left(\frac{\delta I_s}{I_s}\right)^2 + \left(\frac{\delta R_\infty}{R_\infty}\right)^2}$$

Again, for the relative uncertainty of Θ, and thus h, to be low, Θ itself must be high.

To apply these equations to actual sensor system designs is important in evaluating the future potential of underwater hot-film measurements. The uncertainty relations above can be used to determine sensor characteristics (resistance, current, voltage, size), but such design must be done under several constraints. The first constraint is the sensor voltage. To keep a constant current system of manageable size, the number of current sources must be minimized. This requires the sensors to be wired in series in strings of nominally 32 sensors. Smaller strings could be considered, but for a 1000-sensor system, much fewer than 32 is not reasonable. Assuming only 40V of potential is available across any given sensor string (to allow one to use "standard" IC's), that limits individual sensor voltages to the order of 1 volt. Similarly, the maximum current should be limited to several amps for safety and power availability concerns (the total current requirement of the whole system is the maximum current per string times the number of strings). Certainly if this system is ever used in a more remote setting and requires battery power, these power constraints will be tightened further.

The following figures show example uncertainty calculations for a constant current system similar to the one described in this report. For this calculation, the following constraints were imposed. Properties for water at 300°K were used. A 32-sensor string was assumed, so the sensor voltage was limited to a maximum of 1 volt. To maximize sensitivity, a maximum current was calculated for each situation that would result in such a sensor voltage. Therefore, the remaining constraints were sensor design, that being resistance and physical size. To compute the uncertainties, it was assumed that the voltage uncertainty is 0.1 mV, the current uncertainty is 0.1 mA, and the sensor cold resistance uncertainty is 0.001Ω. *It is very important to note that these levels of uncertainties are probably unattainable in practice.* Their values were selected in order to obtain measured uncertainties below 100%. As Figure 32 shows, even with these very low measurement uncertainties, the uncertainty on the film coefficient is no better than 25% for a sensor of the current size. In Figure 33, it is clear that uncertainties can be improved dramatically by decreasing the sensor size, but it is questionable whether the technology exists to make a sensor so small and still retain the low resistance.
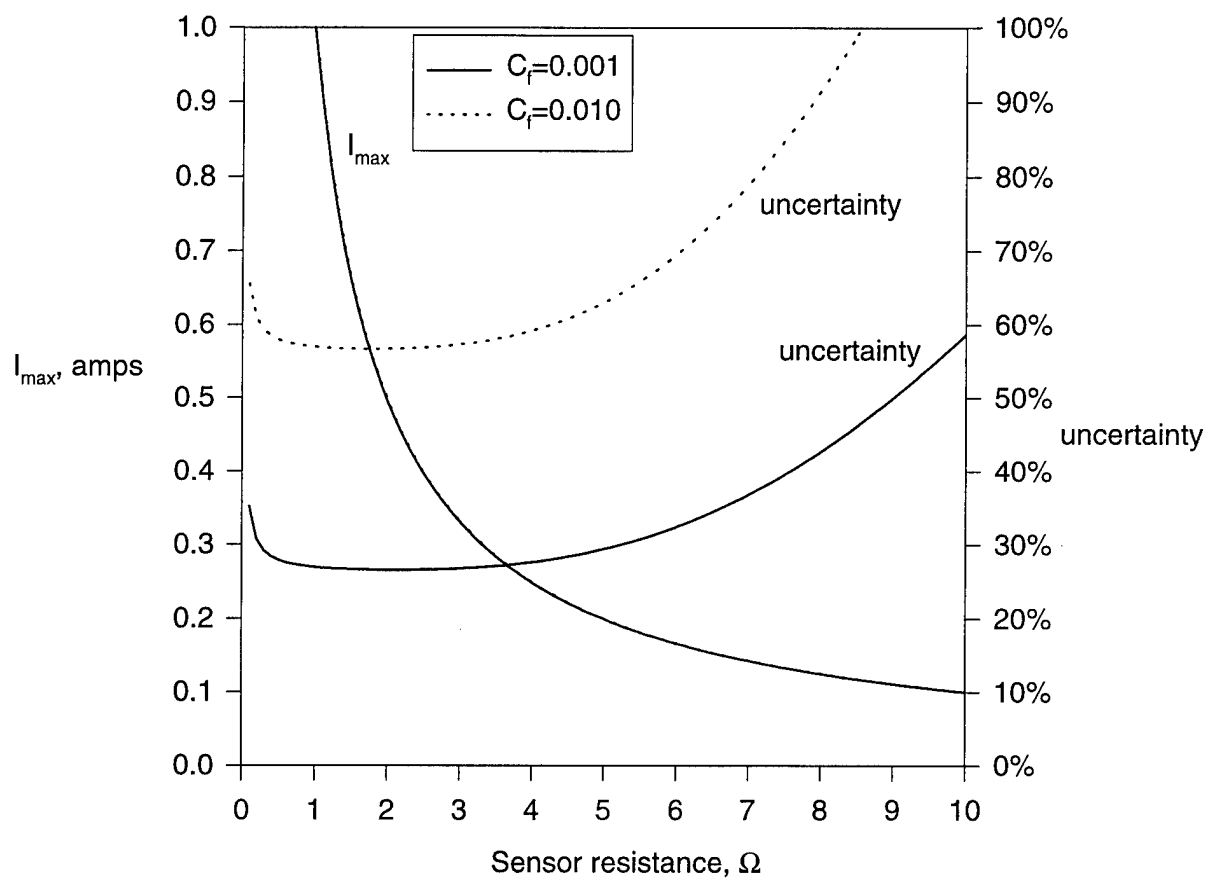
Figure 32. Variation of sensor current and uncertainty with sensor cold resistance for constant current system. Assumes area is same as existing sensor. Maximum sensor voltage of 1V enforced. Fluid properties of water at 300°K are used.
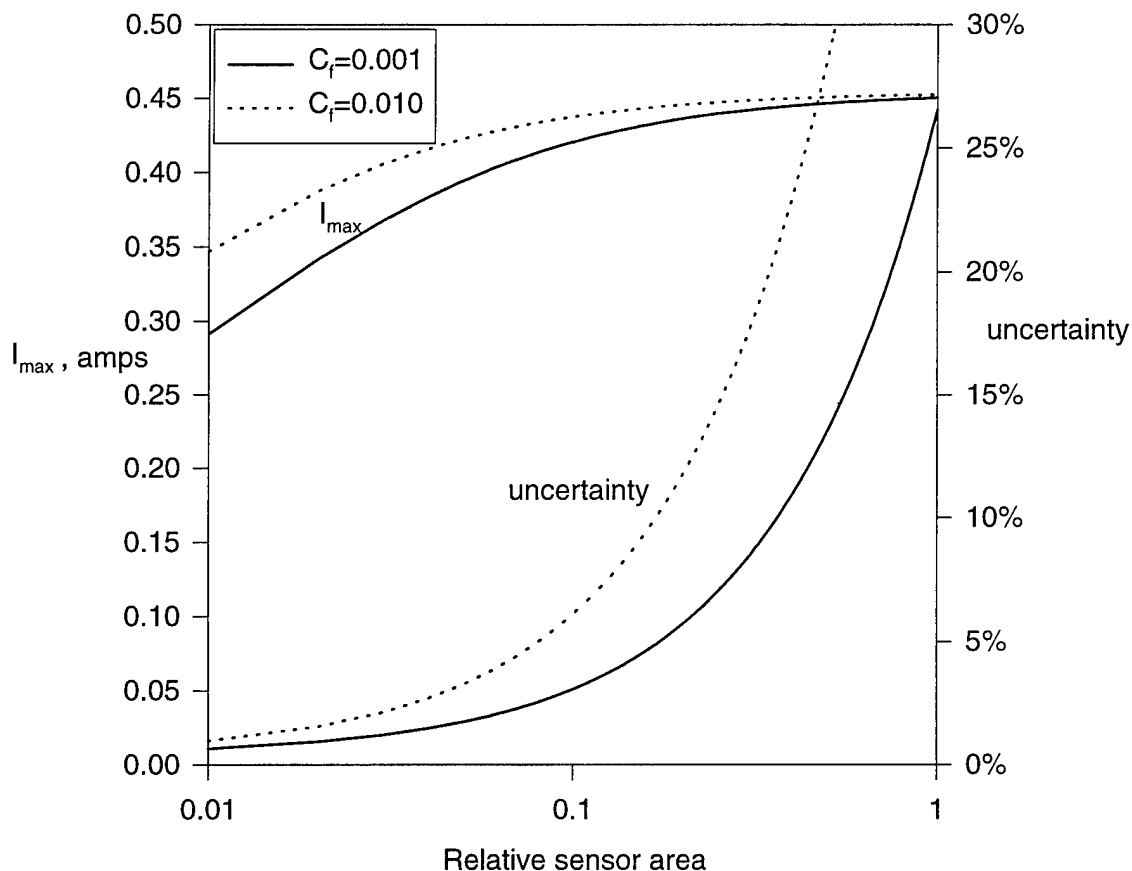
Figure 33. Variation of sensor current and uncertainty with relative sensor size for a constant current system. $R_{inf}=2.2\Omega$. Relative sensor area of 1 refers to existing sensor size ($2.03\text{x}10^{-5}$ m^2). Maximum sensor voltage of 1V enforced. Fluid properties of water at 300°K are used.

Constant Temperature Anemometry

Consider as an alternative a constant temperature bridge arrangement (Blackwelder, 1981). It is important to point out that there are several very good reasons why constant temperature anemometry has been dismissed thus far. In typical constant temperature anemometers there are several adjustments necessary for proper operation, including bridge ratio, over-heat ratio, cold resistance, linearization, bias, etc. In addition, the number of components and leads per sensor would seem to be at least twice as many as are used in the constant current configuration. It would not seem feasible that a 1000-sensor system could be manageable with each sensor requiring all of these adjustments and components. However, for argument's sake, let's examine what could be gained.

A highly simplified constant temperature anemometer circuit is shown in Figure 34. The sensor forms one leg of a bridge, and the resistor in the leg opposite the sensor controls the sensor resistance by unbalancing the

61

bridge, which causes the high-gain op-amp to send more current to the bridge, which heats up the sensor and increases its resistance until the bridge is essentially balanced. Any changes in film coefficient change the heat transfer leaving the sensor. The constant temperature anemometer circuit forces the sensor resistance, and thus temperature, to remain constant, so to compensate for the change in heat transfer due to the change in film coefficient, the op-amp changes the sensor current. The voltage leaving the op-amp is thus a measure of the film coefficient. Bridge circuits are typically used to amplify very small changes in resistance, while constant temperature anemometer circuits are often implemented due to their beneficial increase in system frequency response.
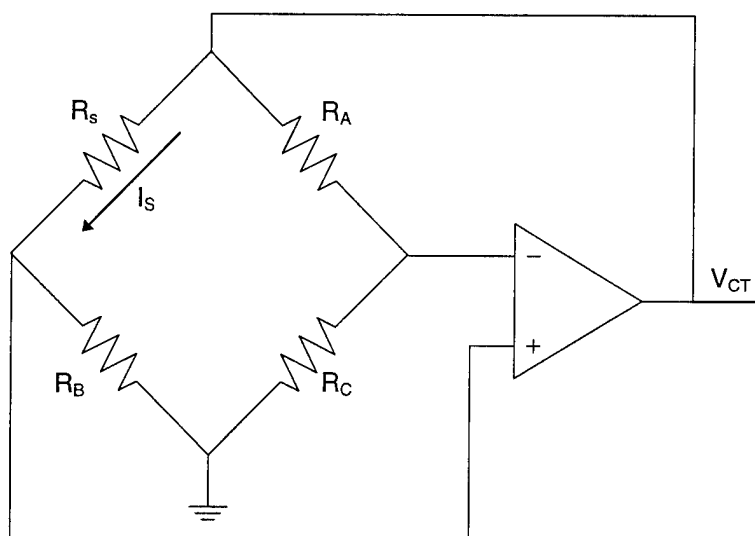

Figure 34. Simplified constant temperature anemometer.

The output voltage as a function of film coefficient can be derived as follows. The sensor current is simply determined from the bridge to be:

$$I_s = \frac{V_{CT}}{R_s + R_B}$$

As was done for the constant current anemometers, one can assume that the Joule heating in the sensor is equal to the heat transfer to the water (neglecting heat transfer to the model), and solve for the output voltage:

$$I_s^2 R_s = hA_s \Theta$$

$$\frac{V_{CT}^2}{(R_s + R_B)^2} R_s = \frac{hA_s}{\alpha}\left(\frac{R_s}{R_\infty} - 1\right)$$

$$V_{CT} = (R_s + R_B)\sqrt{\frac{hA_s}{\alpha}\left(\frac{1}{R_\infty} - \frac{1}{R_s}\right)}$$

$$= (R_s + R_B)\sqrt{\frac{hA_s}{\alpha}\left(\frac{\beta - 1}{R_s}\right)}$$

where β is the overheat ratio, or the ratio of heated sensor resistance to the cold sensor resistance. In this case, the output voltage V_{CT} is a strong function of the film coefficient. The uncertainty calculation in this case becomes easier too, since R_s is determined by the bridge resistances only and does not change from one test to another. Therefore, it is part of a calibration constant, as are all other terms in the equation except the cold resistance R_∞ and the film coefficient h. In fact, if the tests are run in a fluid medium where the fluid temperature is very constant, which is the case at the model basin, then the cold resistance of the sensor will also be a constant, and when evaluating the relative sensor uncertainty, assuming there is some way to calibrate the relative differences out between any two sensors, the only uncertainty playing a role is the voltage uncertainty:

$$C_f = K_1 h^3 = K V_{CT}^6$$
$$\frac{\delta C_f}{C_f} = \sqrt{6}\frac{\delta V_{CT}}{V_{CT}}$$

This uncertainty is very easy to minimize. The key in this bridge configuration is the measured voltage is a strong function of the film coefficient, and thus low uncertainties are easier to achieve.

Low uncertainties are not the only potential benefit. Notice that nowhere in the uncertainty relationships above is there a requirement for the sensor to be run at a high temperature. The beauty of a bridge circuit is it naturally amplifies small changes in sensor resistance. The consequence of this fact is that sensors can now be designed with a much higher resistance and require a much lower supply current. This, in turn, theoretically opens the possibility for very-low-power anemometry for the first time.

In standard anemometry, especially hot-wire anemometry, the sensor's resistance is typically on the order of several ohms due mainly to manufacturing constraints. The current required to drive a bridge with such a low impedance is often much higher than what a typical op-amp is capable of supplying. Therefore, in practical anemometry circuits, the op-amp output is fed through a transistor which behaves like a current amplifier which in turn drives the bridge. Such a configuration would not be feasible to implement in a 1000-sensor system. However, if the sensor resistance were to be on the order of several hundred to a thousand ohms, only milliamps of current would be required to drive the bridge. That being the case, it is theoretically possible for an I/C op-amp to *directly* drive the anemometer bridge. This is implementable, in that it would require 1 op-amp per sensor, which is the same as is currently used in the constant current setup.

To complete the implementation, the bridge would have to be hard-wired in a pre-determined bridge ratio and overheat ratio. This, however, is where the difficulty of implementation comes into play. If one is using very high resistance sensors, then in order to keep the bridge voltage within a reasonable range, the overheat ratio must be very low, resulting in a very low sensor temperature. Again, this does not hurt uncertainties because the output voltage is still a strong function of film coefficient and the circuit is very sensitive to very small changes in heat transfer. However, such very low overheat ratios require extremely well balanced bridges. In typical constant temperature anemometers, resistor R_A is most often a potentiometer. When R_A is too low to heat up the sensor (lower than the sensor cold resistance), the bridge does not function at all. As R_A surpasses the sensor cold resistance, then

the bridge heats up the sensor. For this type of configuration in water, overheat ratios on the order of 1% or less are required. This means that the bridge resistances and the sensor resistance, in order to be effective if hard-wired, must be known to within better than 1%, preferably better than 0.1%. It is easy to guarantee this with the bridge resistances, which can be specified to within +/-0.01% or possibly even better. However, the sensor cold resistance presents a real problem. One problem is the manufacturing tolerance in the sensor resistance. The sensors used in this report have a typical resistance tolerance of around +/-1%. Strain gage manufacturers specify a tolerance of between +/-0.15% and 0.3%. These tolerances are marginal for the intended application. The second, and more severe, unknown on the sensor cold resistance is the change due to the ambient water temperature. The sensor resistance changes by 0.5% per degree Celsius. This means that for a hard-wired, high impedance bridge to be designed properly, the model basin water temperature would have to be known very accurately *apriori*, and this temperature would have to remain very constant. This is an impractical limitation that must be worked around.

There are several possible ways to deal with these problems. In order to improve sensor tolerance problems, if an easy, reliable, and very accurate technique for measuring sensor resistance can be developed, then all sensors purchased in a given batch can be measured and grouped by value. For instance, if the sensors are 100Ω sensors with a tolerance of 0.15%, resulting in resistances from 99.85W to 100.15Ω, then all of the sensors from 99.85Ω to 99.90Ω could be separated into one group, sensors from 99.91Ω to 99.95Ω could be separated into a second group, etc. Then, assuming the anemometers were somewhat modularized into boards serving groups of 16 or 32 or some other small number, all sensors hooked to a given board could be from the same sub-batch of sensors, guaranteeing that the tolerance between all sensors on a given board is smaller than the manufactured tolerance (in this example, the tolerance would be reduce to 0.05%).

This being the case, assuming a very uniform coefficient of resistivity among the sensors, the change in sensor resistance with temperature should be very uniform. Therefore, all bridges for all sensors would need to be adjusted by identical amounts. This can be done by using a D/A converter to inject a specified amount of positive or negative bias voltage into the bridge, thus altering the bridge balance, changing the current flowing to the bridge to balance the circuit, and thus changing the sensor resistance required for bridge balance. This is equivalent to a change in overheat ratio. Therefore, the bridge can be designed to be nominally in balance, and all bridges in a given group will be nominally the same amount out of balance, but a single D/A converter servicing all of these bridges simultaneously can be used to balance the bridge as a measure of the sensor cold resistance at whatever ambient temperature exists and then set the overheat ratio accordingly. A side benefit is now the user does have the ability to use a range of overheat ratios and is not limited to a single, hard-wired overheat ratio.

The following figures show sample calculations of the sensor voltage and current as functions of sensor resistance and size. Water at 300°K is assumed in these calculations, as is an overheat ratio of 1%. Also, the resistances in the legs opposite the sensor (R_B and R_C) are assumed small (~1%) compared to the sensor resistance and the R_A. In these plots, typical bridge currents of 50 mA are reported, which is on the upper end of the capabilities of I/C op-amps (non-power-amps). Efforts must be made to reduce this current to around 20 mA. This can be done by reducing the overheat ratio further, and optimizing the bridge resistances.
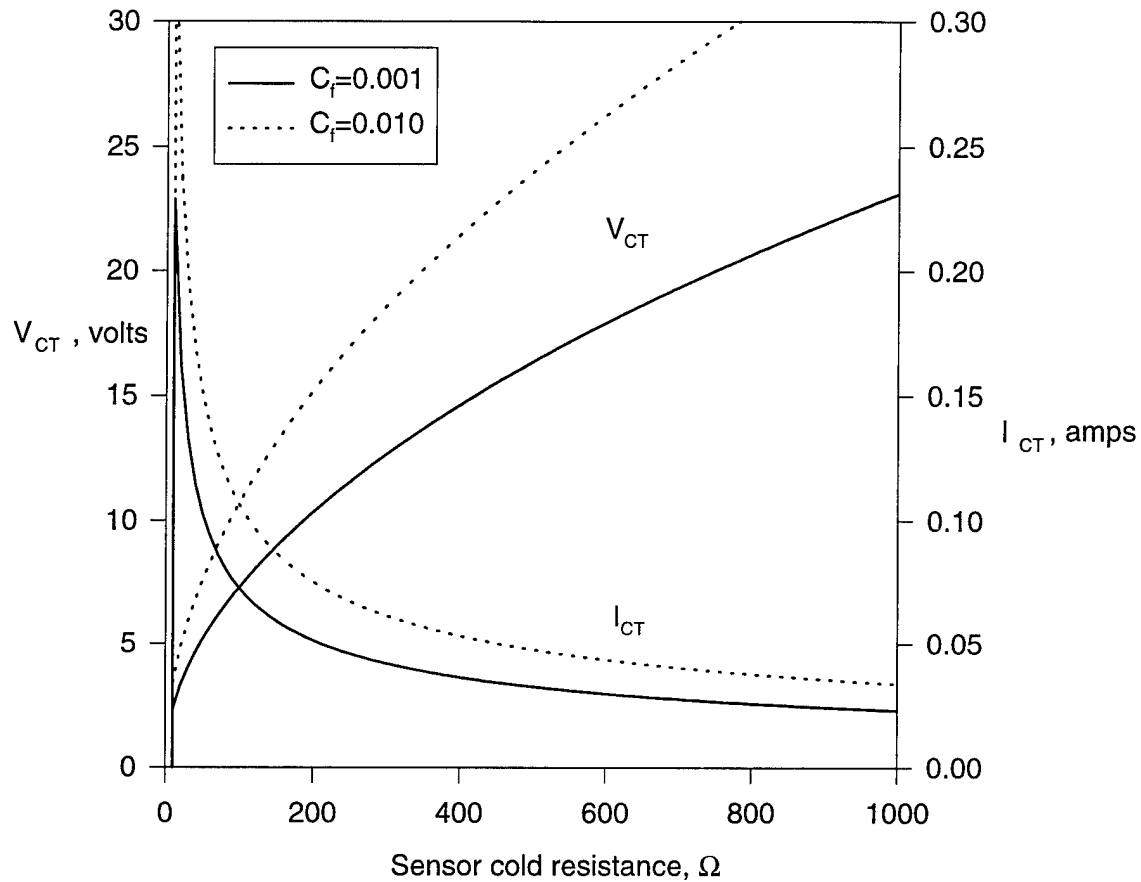
Figure 35. Sensor output voltage and required current for constant temperature system as a function of sensor cold resistance. Water at 300°K assumed. Sensor area is same as existing sensor (2.03×10^{-5} m^2) Overheat ratio of 1% assumed. Assumes bridge resistances in legs opposite sensor is roughly 1% the sensor resistance.
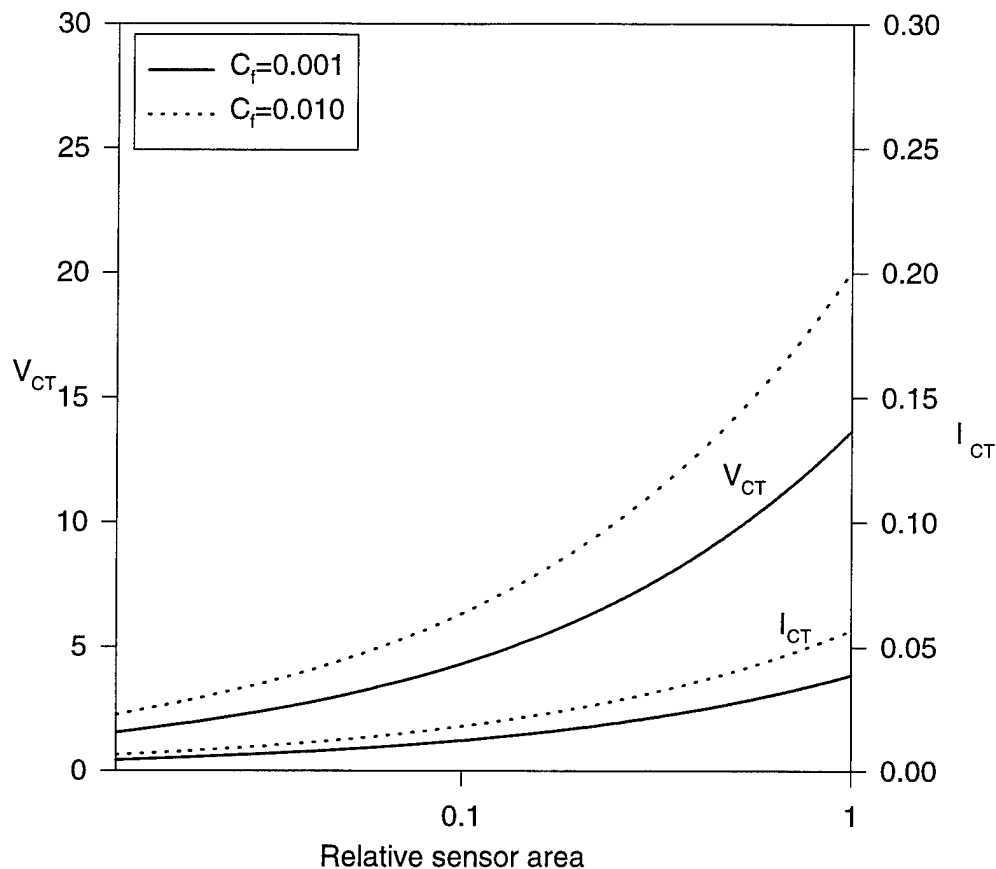
Figure 36. Sensor output voltage and required current for constant temperature system as a function of sensor area. Water at 300°K assumed. Relative sensor area of 1 is same as existing sensor (2.03×10^{-5} m^2) R_{inf} is 350Ω. Overheat ratio of 1% assumed. Assumes bridge resistances in legs opposite sensor is roughly 1% the sensor resistance.

General Results

The purpose of this chapter is not to specify in detail what the hot-film configuration must be, but instead provide some new ideas and directions that address the existing problems and to evaluate how feasible a solution is. In addition, it is felt that an effective design is one that is not only applicable to the rotating arm tests described in this report, but is more importantly applicable to tests in radio-controlled models (RCM's), where power and space limitations are dominant.

Regardless of what type of anemometry circuitry is used, it seems that smaller effective sensor area is a direction that must be pursued. Smaller sensor area makes the sensor a much more efficient heater, allowing for higher levels of heat transfer and thus more sensitive measurements. Sensor area should be decreased by at least one order of magnitude, which would require a sensor diameter roughly one third that of the existing sensor. The smallest strain gages are almost three orders of magnitude smaller (for example, Measurements Group 008CL, sensor dimensions are 0.20mm by 0.25mm for an area of 5×10^{-8} m^2, or 0.25% of existing sensor size). It is important to note that smaller sensors are more fragile, more susceptible to burnout from thermal shocks at power up, more expensive,

and more difficult to manufacture with tight tolerances. As always, any new sensor geometry design will require weighing all of these tradeoffs very carefully in conjunction with the sensor manufacturer to settle on a suitable balance of traits.

For any system where the goal is to run a very large number of sensors simultaneously, the labor per sensor in terms of calibration, data acquisition and reduction must be minimized without compromising the precision of the data. This means that all components specified should be very high precision. This includes all resistors and amplifier circuits. Also, it is very desirable to minimize the number of measurements necessary. This is a major part of the attraction of the constant temperature configuration, which requires one voltage to be measured per sensor only, as opposed to the constant current measurements which currently require the cold resistance and sensor current to be known with precision in addition to the sensor voltage.

Conclusions

A very ambitious program to measure surface shear stress at 1000 locations on an underwater body failed to provide data but resulted in very significant technological advances and experience that is extremely valuable towards achieving the 1000-sensor system goal. Sensor installation is described in detail, including wiring and waterproofing and the various issues encountered during that labor-intensive project component. The electronics system is documented in detail, with particular reference to how each sub-circuit is calibrated or was modified to optimize its accuracy. The software which acquires, reduces, and organizes the voluminous amounts of data associated with such a system is also documented, along with the data reduction schemes and an uncertainty analysis. Two model basin entries are described along with the problems encountered and the significant solutions and advances made during each. The failure of the existing system is attributed to improperly scaled sensor current. A detailed examination is made as to what changes would need to be made in order to get a similar system to work, and what alternative systems will work in place of constant current anemometers. It is shown that the sensor size should be reduced as much as possible, and the resistance should be raised to reduce the current requirements of the system. Constant temperature and constant voltage anemometers are proposed as possible alternatives to the constant current anemometers. In any case, a detailed design study should be pursued before constructing any new anemometer hardware, and more exhaustive small-scale tests should be done before attempting full-scale measurements.

Acknowledgments

References

Blackwelder, R. F., "Hot-Wire and Hot-Film Anemometers", *Methods of Experimental Physics: Fluid Dynamics*, vol. 18, part A, pp. 259-314.

Simpson, R.L., Walker, D.A., and Shinpaugh, K.A., *Description of a 1000 Sensor Constant Current Anemometer System for Locating Three-Dimensional Turbulent Boundary Layer Separations*, Virginia Polytechnic Institute and State University, Aerospace and Ocean Engineering, Report VPI-AOE-185, 1991.

Wetzel, T.G., *Unsteady Flow Over a 6:1 Prolate Spheroid*, Dissertation, Virginia Polytechnic Institute and State University, Aerospace and Ocean Engineering, 1996.

Appendix A

Interim Report: Waterproofing Hotfilm Sensors for Underwater Use

Todd G. Wetzel

Roger L. Simpson

Virginia Tech

Aerospace and Ocean Engineering

Blacksburg, Virginia

June 5, 1995

Introduction

During the original phase of this research project several years ago, the initial sensor design used in tests in a towing tank at DTRC called for sensors covered in a 0.001" thick waterproof layer of Kapton plastic film. The newer sensor design, used in the present tests, called for no covering on the sensors. The intent was to install a covering during installation with a lower "thermal thickness" than the original 0.001" Kapton. MasterBond EP21ANLV was specified because it has a thermal conductivity on the order of 10 times higher than Kapton and most other epoxies and coatings. However, when it became time to use it in the present installation, problems were found with the MasterBond. First, it required an installation thickness of at least 0.010", 10 times thicker than the original Kapton. Second, it did not adhere properly to the model surface. This was probably due to inadequate surface preparation. Therefore, most of the MasterBond was stripped off the model. In a few places, the MasterBond adhered well enough to prevent stripping it off without damaging sensors, so it was left on. Fiberglass gelcoat was then selected because it was readily available and was intended for use on boat hulls, thus making it an appropriate choice for use underwater. Three coats of gelcoat were brushed on all of the sensors, including the ones with the MasterBond on them. This resulted in a rough, but hopefully watertight, surface.

During the ensuing Rotating Arm entry at the Model Basin, it was found that the water proofing applied to the sensors was entirely inadequate. This lack of waterproofing led to the following modes of failure:

- Current leaked into the water which eventually led to current source runaway and sensor burn out.
- Large amounts of corrosion formed quickly on the copper foil sensor interconnects and solder joints.
- Some of the adhesives broke down in isolated locations.

These failures resulted in making the entire system unusable, since sensors are connected in series and one failing sensor results in a string of 31 sensors becoming inoperable. In all, on the order of 20 sensors burned out in over 1 hour of rigorous running of the sensors. It was determined at that time that the waterproofing problem could not and should not be solved quickly and haphazardly, but instead should be re-examined very carefully in order to maximize the chance of success in repairing or replacing the sensors.

This interim report describes waterproofing tests that were conducted at Virginia Tech. Included are descriptions of potential repair scenarios, issues that needed to be examined, test that were performed, sample data that were collected, and final summaries of things learned and future action to take.

Changes Made in Addition to Sensor Repairs

During the time that the waterproofing tests were being performed, several other system improvements were being implemented in parallel.

New Electronics Housing

The Plexiglas housing originally designed did not perform well at the Model Basin. The complex shape gave rise to leaks in hard-to-seal corners. The use of a silicone-type sealant meant it would take a day at least of letting the lid seal cure before being able to submerge the box. It also made removal of the lid messy and time

consuming. Also, the threaded holes for the lid screws all cracked. In addition, one of the PVC unions that serve as entrance ports for the signal cables developed a leak due to an undersized adhesion surface between it and the box.

Since the box has been moved to the nose and there is no longer a sting constraint on it, a new box with a simpler geometry has been designed and is currently being built. The new box is made out of aluminum to make it strong and durable. All bolt sizes have been increased from 10-24 to 1/4-20. The shape is rectangular. The lid is sealed with a gasket instead of a silicone adhesive. The PVC unions are now fit much more securely over a much wider area. Plus, there is now much more room on the inside of the box for connecting all of the cables.

Sealing Where the Individual Wires Penetrate the Model Skin

There was some concern that the wires that penetrate the model skin are not adequately sealed to prevent water leaking to the sensor from the back. While we have had no known problems of this sort, it is also extremely difficult to detect a leak like this. Therefore, to be safe, the wire waterproofing will be further augmented as described below in *Proposed Repair Procedures.*

Repair Scenarios

The damage to the sensors system was extensive. Upon very close inspection of the sensors on the rear lid of the model, which contained 25% of the sensors used, it was found that on the order of 75% of the sensors showed signs of one or more modes of failure as described in the introduction. Therefore, the first possible repair scenario is to replace all of the sensors outright and use a completely new waterproofing technique. This scenario would incur a huge expense in both time and money but would also provide for a chance to improve the entire installation quality. A second scenario would involve replacing only the sensors that were fully damaged, carefully cleaning all of the sensors, and applying a new covering over top of the existing coatings. This would be lest costly in both time and money, but risks robustness in that failed materials are left behind on the sensors, which may not only adversely affect adhesion but also will lead to a thicker buildup of material over the sensors, cutting down on sensitivity. The second scenario is preferred, however, due to its lower cost, and was investigated first.

Waterproofing Issues and Possible Materials

The original specification for a waterproof coating for these sensors was for a material that is water tight and "thermally thin", or has a high thermal conductivity. These are extremely difficult conditions to meet. However, in this case, the thermal conductivity requirement is going to be relaxed. The covering on the sensor mostly affects the frequency response of the sensor and only secondarily affects its sensitivity. Therefore, a little sensitivity is sacrificed to guarantee proper waterproofing.

Model Basin personnel in the Structures Group suggested a rubber-like material called PR-1005-L made by Products Research and Chemicals Corporation (PRC). They use this product to protect strain gages in underwater applications. The Structures Group even loaned us a pint of the PR-1005-L since it would take 4 to 6 weeks for us to get a pint of our own. The PR-1005-L is typically brushed on. Brushing, however, leaves brush marks and makes it difficult to get full coverage with thin coats, even when using multiple coats. The PR-1005-L can be sprayed, but it is

difficult to do so and requires a fairly expensive spray gun. Otherwise, the PR-1005-L exhibits excellent adhesion and is translucent, so the sensor is visible at all times.

When researching spraying options for the PR-1005-L, it was recommended to look into Spray Tool Dip, which is a rubber coating similar to the PR-1005-L, but it comes in a spray can. This product seems to exhibit properties similar to the PR-1005-L except that it is not translucent. However, the spray can allows thin, even applications with better coverage. These are the two materials that were investigated for repairing the sensors.

Waterproofing Tests

Initial Setup

A 6" diameter PVC pipe was coated with a fiberglass gelcoat to simulate the geometry and surface of the submarine model. This model was fitted with three rows of 9 sensors each, with the sensors spaced every 22.5° over a 180° span. The sensors were installed exactly as they were originally installed on the submarine model. They were waterproofed initially with only the same gelcoat as was used on the submarine model. Every step of the original submarine installation was simulated including surface preparation.

Gelcoat Waterproofing Tests

The pipe was then submerged in a 2'x2' water tunnel. The resistance was checked between a conductor on the sensor cable and the water, and the resistance was found to be on the order of $k\Omega$s, which indicated that the gelcoat waterproofing was not working at all. The sensors were run in this configuration for 5 hours in order to force sensor failure. Unlike in the experience at the Model Basin, no sensors burned out. The researchers speculate that this is due to a lower ion concentration, and thus a lower conductivity, of the water used in this water tunnel compared to the water in the Model Basin. Some attempts were made to increase the water conductivity in the tunnel, but this was not pursued very far for fear of damaging the water tunnel hardware. The sensors also seemed to work properly in that they responded to changes in supplied current. However, when data were taken on the cylinder in a 30° incline at speeds of around 20 cm/s, the data were horrible.

This test led to a discovery of a good way to test the effectiveness of the waterproofing on-line. As a review of the way the data are reduced, the voltage and the current for each sensor are computed from the raw voltages measured. These data are used to compute the heat transfer into the water ($\dot{q}$) and the temperature difference between the sensor temperature and the water temperature ($\Theta = T_f - T_{inf}$). The sensors are run at several currents which results in several ($\dot{q}$, Θ) pairs which are fit with a regressed line to get a film coefficient h, which is ultimately proportional to skin friction. When the regression is performed, a correlation coefficient, R^2, is computed as a measure of the linearity of the regressed line. Of course, the closer R^2 is to 1.0 the better the fit. Typically in the wind tunnel data which was successfully taken in June of 1994 these correlation coefficients ranged from 0.9990 to 0.9999. In the initial water tunnel tests when the water proofing was not effective, the correlation coefficients were on the order of 0.4, which means the sensors were not behaving properly at all.

Application of New Waterproofing Materials

Next the sensors were dried and cleaned and the new waterproofing materials were applied *on top of the existing gelcoat.* This was done to see if it is possible to repair the sensors without replacing them. Two coats of the PR-1005-L were brushed on one ring and two coats of the Spray Tool Dip were sprayed on the other two rings. The measured resistance between the sensor conductors and the water went up considerably as did the correlation coefficients. By visually inspecting the sensors very carefully and using the correlations as a diagnostic, several iterations of locating potential leaks and touching them up led to the waterproofing-to-water resistance going to over 10MΩs and the correlation coefficients ranging from 0.99 to 0.999. The data acquired then made physical sense and indicated separation properly.

These tests indicated that it was possible to overcoat the existing sensors and get them to not only be waterproofed but also to remain sensitive. The pipe is currently being stored underwater indefinitely to track the long term behavior of the Spray Tool Dip to underwater conditions. So far its adhesion and solidity has not deteriorated at all.

Sample Data

Included in the following figure is sample data taken on the pipe in a normal to the flow, semi-infinite cylinder configuration at a Reynolds number of 29,000. To account for the differences in sensitivities of the different sensors in a given string, the sensors are scaled to each other such that the "leading edge" sensor has a value of "1.0". The y-axis is a value proportional to wall shear. The x-axis represents the circumferential position of a given sensor in degrees, with 0° corresponding to the windward side of the pipe and 180° corresponding to the leeward side. A minimum in wall shear indicates separation. The data is presented for three rings. Because of the length of the pipe, these three rings were close to the free surface of the water tunnel (Ring 3 was about 2" from the free surface, Ring 2 about 4", and Ring 1 around 6"), so there is probably some three-dimensionality in the flow where the sensors are located. Despite this fact and the fact that the sensors are spaced out rather coarsely (every 22.5°), it is still clear that the separation is occurring around 90°. This is consistent for standard, low Reynolds number flow around a cylinder. In the model basin tests, where the flow speed is more than an order of magnitude faster than in these tunnel tests, the variation in wall shear will be larger and the sensors should respond even more clearly. Plus, the special resolution will be improved to every 5°.
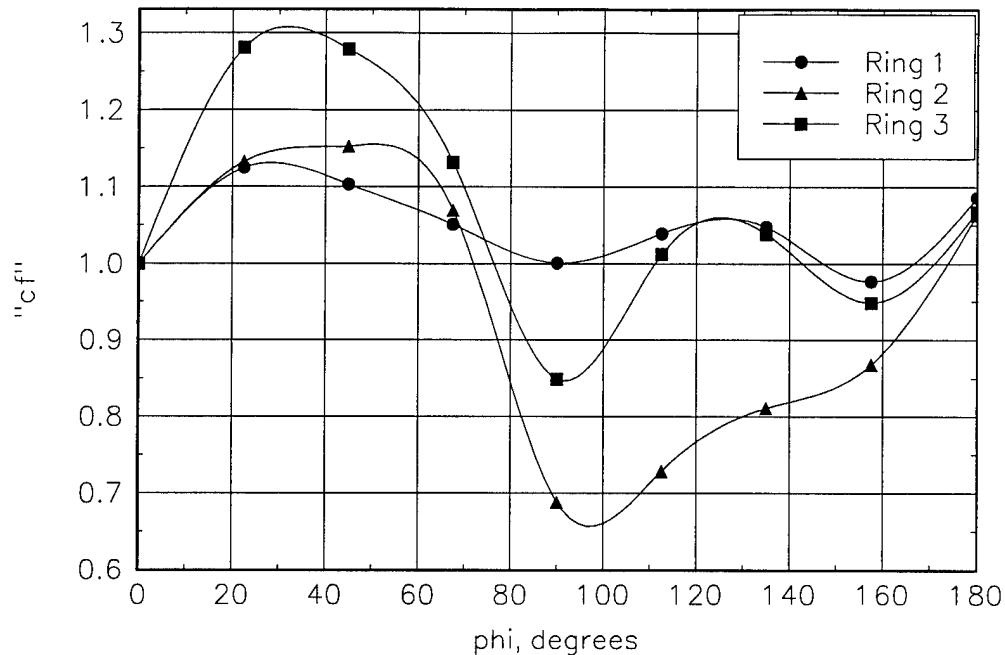
Figure 1. Wall shear distributions for cylinder test done in water tunnel at Virginia Tech. Splines drawn for visual aid only.

Proposed Repair Procedures

The following procedure is recommended for repairing the existing sensors:

1. Replace all burned out sensors.

2. Remove all loose gelcoat. Some sensors had bubbles form on them and it was originally intended to replace these sensors. Instead, just remove these bubbles of gelcoat from the affected sensors carefully.

3. Search for places where the copper foil is sticking up. Try to clean up any of these sharp edges.

4. Test all sensors with the electronics to verify that there are no other sensors that need to be replaced.

5. Very thoroughly clean all sensors at least twice with Methyl Ethyl Ketone, being careful to apply the solvent with one rag and wipe it up with another. Use a hair dryer to remove any excess MEK to minimize absorption into the fiberglass.

6. Spray the copper foil interconnects with 2 coats of spray adhesive. Use a piece of cardboard as a temporary mask to prevent covering the sensing areas. Hit trouble areas with extra thick coatings.

7. Spray 2 additional coats on all of the sensors, including on the sensing areas.

8. Spray 4 coats on the inside of the model, where the individual wires penetrate the model skin. Be especially careful to fully penetrate in between all of the wires.

9. Dip the model piece by piece into the water. Check for resistance between the water and the conductors. For any rings with particularly low resistance, inspect the sensors and look for potential trouble spots.

10. Take and reduce data to get correlation coefficients. Use as a diagnostic to help locate waterproofing leaks.

11. Iterate steps 9 and 10 with additional coats of Spray Tool Dip where needed.

12. When all parts are adequately waterproofed, apply 2 coats of Thompson's Water Seal (separated by 24 hours) over all sensors, inside and out. Allow to cure an additional 48 hours before submerging in the water.

Following this procedure, we should be able to proceed with the tests at any time with confidence.

The primary time constraint for completing this list is the cure time of the coatings, particularly the Thompsons Waterseal. It is estimated that, with a workforce of 2 Virginia Tech Students, the model could be repaired in 1 week, with a second week available for backup in case of further complications. Given the present schedule on the arm, however, which prevents the tests from being attempted again until September, it is recommended that the model be returned to Virginia Tech so a more careful and thorough job can be done in repairing the sensor system.